FFI RAPPORT

RUMBLE PROJECT
SCATTERING INDEX MODELS

JENSERUD Trond , FFIBM, NO
SIMONS Dick, TNO-FEL, NL
CRISTOL Xavier, TMS, FR

FFI/RAPPORT-2001/03685

FFIBM/821/116

Approved
Horten 12. September 2001

Tor Knudsen
Director of Research

RUMBLE PROJECT
SCATTERING INDEX MODELS

JENSERUD Trond , FFIBM, NO
SIMONS Dick, TNO-FEL, NL
CRISTOL Xavier, TMS, FR

FFI/RAPPORT-2001/03685

FORSVARETS FORSKNINGSINSTITUTT
Norwegian Defence Research Establishment
P O Box 25, NO-2027 Kjeller, Norway

FORSVARETS FORSKNINGSINSTITUTT (FFI)
Norwegian Defence Research Establishment

P O BOX 25
N0-2027 KJELLER, NORWAY

UNCLASSIFIED

SECURITY CLASSIFICATION OF THIS PAGE
(when data entered)

REPORT DOCUMENTATION PAGE

1) PUBL/REPORT NUMBER	2) SECURITY CLASSIFICATION	3) NUMBER OF PAGES
FFI/RAPPORT-2001/03685	UNCLASSIFIED	55
1a) PROJECT REFERENCE	**2a) DECLASSIFICATION/DOWNGRADING SCHEDULE**	
FFIBM/821/116	-	

4) TITLE

RUMBLE PROJECT
SCATTERING INDEX MODELS

5) NAMES OF AUTHOR(S) IN FULL (surname first)

JENSERUD Trond , FFIBM, NO
SIMONS Dick, TNO-FEL, NL
CRISTOL Xavier, TMS, FR

6) DISTRIBUTION STATEMENT

Approved for public release. Distribution unlimited. (Offentlig tilgjengelig)

7) INDEXING TERMS

IN ENGLISH:	IN NORWEGIAN:
a) Backscattering	a) Tilbakespredning
b) Roughness	b) Ruhet
c) Volume inhomogeneities	c) Voluminhomogeneiteter
d) Perturbation methods	d) Perturbasjonsmetoder
e) Seafloor	e) Havbunnen

THESAURUS REFERENCE:

8) ABSTRACT

In this note we describe some models for the backscattering strength of a rough seafloor. The models range from the simple Lambert's rule to perturbation models that include the effect of roughness and volumeinhomogeneities.

For grazing angles in the range say 5-40^0, the dependence of backscattering strength on grazing angle can in many cases be described by Lambert's rule. To obtain good correspondence with observations outside this range of angles, it may be necessary to include modifications to the Lambert's rule: At lower grazing angles to include the effect of scattering by volume inhomogeneities, and near normal incidence to include the coherent component. If we want to relate the backscattering strength to physical parameters of the seafloor, it is necessary to use physical models. Two such models are included: A first order perturbation models for roughness scattering, and a first order perturbation model for volume scattering.

A collection of information about roughness and topography of seafloors is also included.

9) DATE	AUTHORIZED BY	POSITION
	This page only	
12. September 2001	Tor Knudsen	Director of Research

ISBN 82-464-0660-4

UNCLASSIFIED

SECURITY CLASSIFICATION OF THIS PAGE
(when data entered)

CONTENTS

BOTTOM SCATTERING INDEX MODELS OF VARIOUS COMPLEXITY

1 INTRODUCTION

The scattering of acoustic waves from the ocean bottom is important for many sonar applications, and has therefore been extensively studied, both experimentally and theoretically.

The problem is complicated: Scattering is caused both by the roughness of the water-sediment interface and by inhomogeneities within the sediment volume. In addition shear waves, interface waves and slow waves may be generated during the scattering process. The scattering mechanisms may also be coupled, and multiple scattering may take place. Studying the effects of all the scattering mechanisms mentioned above requires advanced numerical models such as finite element or finite difference. However, for many applications models which include only some of the scattering mechanisms will be sufficient.

A bottom scattering model usually estimates the surface or volume scattering coefficient as a function of incident/scattering angles, frequency, bottom geoacoustic parameters, and parameters describing the surface roughness and volume inhomogenities. Scatter models can be empirical or physically based.

Empirical versus physical models. Empirical models have the disadvantage that they are not derived from physical processes such that the backscattering strength can not be related to seafloor parameters. A physically based model, however, can be used to extrapolate measured data to unmeasured angles, frequencies and bottom types. A scattering model should preferably relate scatter strength to measurable parameters of the seafloor.

Methods for roughness scattering. Models of various levels of sofistication have been developed. The simplest model is the Lamberts rule, which assume isotropic scattering. Several extensions and modifications to the Lamberts rule have also been developed which remedies some of its shortfalls.

For a surface where the roughness amplitude is small compared to the acoustic wavelength, perturbation theory is valid. Although most work has been on pressure release and ideally rigid boundary conditions, which is not appropriate for seafloor scattering, perturbation theory has been applied to fluid-fluid and fluid-solid boundaries.

For surfaces where the roughness is not small compared to a wavelength, but which are gently undulating, the Kirchhoff approximation is valid.

Some surfaces are rough on many scales. For such surfaces it may be that neither the Kirchhoff nor the Perturbation method is valid, and composite (two-scale) models that combine both approximations into one model are required.

Both Perturbation and Kirchoff methods ignore the effects of multiple scattering at a rough

surface. Approximative methods are developed, which sum contributions from distributions of protuberances to simulate the effect of multiple scattering.

When multiple scattering and shadowing becomes important, which happens for large roughness and grazing incidence, the composite models also fail, and full wavemodels are required.

Volume scattering, joint roughness and volume models. In many cases the scattering by subseafloor structure contributes significantly, and may even dominate the backscattering. A number of researchers have developed volume scattering theories for the bottom. There are also models that accounts for both roughness and volume inhomeogeneities, but does not include multiple scattering.

2 MODIFIED LAMBERT'S RULES

The Lambert's rule is a reasonable description of backscattering for grazing angles between about $5 - 40^0$. But for larger grazing angles, Lambert's rule does not follow observed backscattering strengths (too low values near specular direction), except for very rough surfaces. To remedy this, it is possible to add to the Lambert's rule a term that gives a better description of the field near the specular direction.

For some bottom types, Lambert's rule shows considerable deviations from observations also at low grazing angles (too low values). Again, this can be remedied by for example adding a threshold.

We will now briefly present Lambert's rule as well as the extensions mentioned above.

2.1 Lambert's rule

The variation of scattered intensity with direction depends on the nature of the surface. If the intensity radiated from the surface is independent of direction, then the radiation is said to be isotropic. For isotropic scattering, the scattered intensity I_s is related to incident intensity I_I by [1], p.152

$$I_s = \mu I_I \ \sin\theta \sin\phi \tag{2.1}$$

where θ and ϕ are incident and reflected grazing angles respectively, and μ is a constant. This relation is called Lambert's rule.

For backscattering $\phi = \theta$ and the scattering cross-section becomes

$$\sigma_b(\theta) = \mu \ \sin^2\theta \tag{2.2}$$

where μ is the Lambert constant, which can be interpreted as backscatter strength at normal incidence.

The model depends on only one parameter, μ. The model is frequency independent.

The value of the coefficient μ depends on the bottom type. Mackenzie [2] found that a value of $10 \log_{10} \mu$ = -27 dB fitted his data (530 and 1030 Hz) well. Several later studies have determined μ for different sediment types, see e.g. Garlan [3], from which table 2.1 is obtained

Sediment type	μ (dB)
Rock	-18
Sand	-31
Silt	-37

Table 2.1: Scattering parameter μ for different sediment types [3]

Comment. Lambert's rule assumes totally diffuse scattering, i.e., is valid for very rough surfaces (roughness is large compared to the wavelength). The Lambert's rule lacks a coherent scattering component. This is consistent with the assumption on which the model is based: the coherent field is negligible for very rough surfaces. However, Lambert's rule is often applied to surfaces which can not be characterized as very rough, in which case the lack of a coherent component limits the valid range of the model near specular direction.

The Lambert's rule also often fails to fit data at lower grazing angles, as we will discuss below.

The Lambert's rule can be extended to a general three-dimensional scatter law by assuming symmetry about the vertical direction as well as horizontal isotropy [4].

Lambert's rule gives reasonable agreement with data for heavily ridged bottoms for grazing angles between about $5-40^0$ [5] (which is expected from the theoretical basis for the model). For grazing angles exceeding 40^0 observed backscattering strengths show a strong rise with increasing angle, which is in accordance with perturbation theory, but not with Lambert's rule[6].

We also note that perturbation theory yields a sin^4 dependency of backscatter for small grazing angles [6] and [7] while Lambert's rule suggests a sin^2 dependency.

Lambert's rule appears to be a good approximation to data for many deep water bottoms at grazing angles below about 45^0 [8]

2.2 Lambert-Mackenzie

From measurements bottom scattering has been found to be a function of $\sin^n \theta$ where n is a number between 1 and 2 [2].

$$\sigma_b(\theta) = \mu \, \sin^n \theta \tag{2.3}$$

This generalization of the Lambert's rule is often termed Lambert-Mackenzie scattering in the litterature.

The model depends on two parameters, the Lambert constant μ and the exponent n. The model is frequency independent.

Comment. For $n = 2$ we have the conventional Lambert's rule. The Lambert-Mackenzie model represents a generalization to Lambert's rule, but without any physical basis. The motivation for the rule seems to be that a better fit with measurements can be obtained by allowing n to be a free parameter. The effect of varying n is shown in figure 2.1.

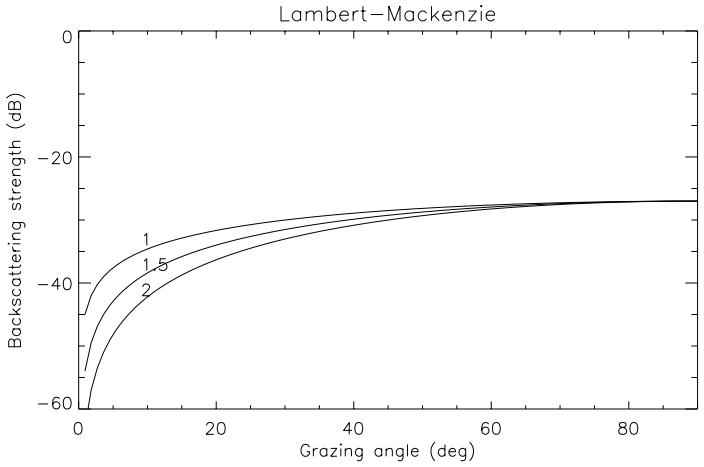

Figure 2.1: Lambert-Mackenzie rule for $\mu = -27$ and n=1,1.5 and 2. The value $n = 2$ corresponds to Lamberts rule.

2.3 Lambert's rule with threshold at low grazing angles

According to Lambert's rule the backscatter strength approaches zero for low grazing angles. In some areas a different behaviour is observed [9], where the backscatter strength approaches a threshold for grazing incidence below some 20^0.

To account for this effect, the Lambert's rule can be modified by adding a threshold, σ_0.

$$\sigma_b(\theta) = \sigma_0 + \mu \, \sin^n \theta \tag{2.4}$$

The model depends on three parameters, the Lambert constant μ, the threshold σ_0 and the exponent n. The model is frequency independent.

Comment. This behaviour can be given a physical explanation. It is probably caused by scattering from inhomogenities within the sediment volume. Volume scattering at low grazing angles will take place for slow sediments, where there is penetration down to low grazing angles (or there may be no critical angle), and subsequent backscattering from the volume.

Figure 2.2 shows the effect of varying the threshold, σ_0, in the modified Lamberts rule.

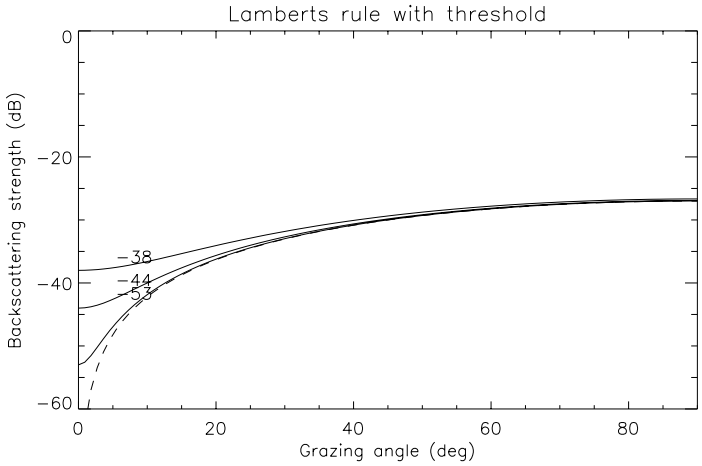

Figure 2.2: Lamberts rule for $\mu = -27$ dB and with different values of threshold, σ_0 = -38, -44 and -53 dB. Dashed line shows Lamberts rule without threshold.

2.4 Del Balzo's rule

The model of Del Balzo [10] is a modified Lambert's rule which includes a correction at low grazing angles. The modification accounts for the effect mentioned above: that in some sediments there exists a scattering-strength platau caused by scattering inside the sediment. But contrary to the previous section, the threshold is not a free parameter, but is connected to the Lambert constant μ. The rule is formulated as

$$\sigma_b(\theta) = \alpha(\phi) + \mu(\phi)\,\sin^2\theta \tag{2.5}$$

where α is the low grazing angle platau, and where both α and μ depend on bottom type through a parameter ϕ. The parameter ϕ is related to the mean sediment grain-size δ in mm by $\delta = (1/2)^\phi$.

Table 2.2 gives the values of grain-size parameter ϕ, lower platau α and Lambert's coefficient μ for some sediment types, based on measurements in the frequency range 300 to 1500 Hz.

Sediment type	δ (mm)	ϕ	α (dB)	μ (dB)
Coarse Sand	0.500	1	-38	-23
Fine Sand	0.125	3	-41	-26
Silty Sand	0.044	4.5	-44	-29
Sand-Silt-Clay	0.016	6	-47	-32
Clayey Silt	0.008	7	-50	-35
Silty Clay	0.003	8.5	-53	-38

Table 2.2: Del Balzo's scattering rule [10]

The model is characterized by only one parameter, the grain-size parameter ϕ. The model is frequency independent.

The backscattering strength as a function of ϕ is shown if figure 2.3.

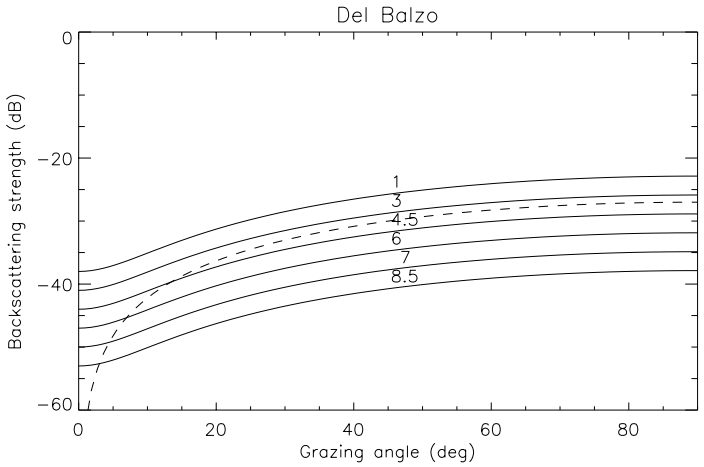

Figure 2.3: Del Balzo rule for different values of the parameter ϕ. The dashed line shows Lamberts rule with $\mu = -27$ dB.

3 MODELS INCLUDING THE COHERENT COMPONENT

The total field can be written as a sum of a coherent, I_{coh}, and an incoherent, I_{inc}, field component.

$$I_T = I_{coh} + I_{inc} \tag{3.1}$$

Let the scattered field due to a plane incident wave be $p(\vec{\mathbf{r}})$. Then the coherent intensity is defined as the square of the expected value of the scattered field, $I_{coh} = |\langle p \rangle|^2$, and the incoherent intensity is the mean *intensity* of the scattered field, $I_{inc} = \langle |p - \langle p \rangle|^2 \rangle$. The incoherent field is often termed the diffuse component because of its wide angular spread and lack of phase relationship with the incident wave, while the coherent field is sometimes called the specular component [11].

The coherent component can be written as $I_{coh} = R_I I_0$ where I_0 is the reflected intensity from a plane interface, and R_I is the coherent intensity reflection coefficient, i.e. the loss due to roughness. The specular peak is due to the coherent component. The specular peak has a finite angular width due to either a finite width incident beam or a finite size of the scattering surface.

Now, it remains to find proper models for the coherent and incoherent components.

3.1 Ellis' model

None of the models described so far can be used near the specular direction. Ellis [4] describes a 3D bistatic scattering function which is valid both for diffuse and specular scat-

tering. The model combines the Lambert's rule for diffuse scattering and a facet model for specular scattering into one model. For backscattering the cross section becomes

$$\sigma_b(\theta) = \mu \, \sin^2\theta + \nu \, \frac{1}{\sin^4\theta} \, \exp\left(-\frac{\cot^2\theta}{2\sigma^2}\right) \tag{3.2}$$

Here μ is the Lambert constant, ν is the facet strength, and σ is the rms facet slope. The latter term is sometimes called a facet width since it is a measure of the angular width near normal incidence over which the facet reflection process is important [4].

The model depends on three parameters, μ, ν and σ that can be fit to measured backscatter data. A best fit to measurements at a deep water location gave the following values [4]: $10\log\mu = -32$ dB, $10\log\nu = -12$ dB, and $(180^o/\pi)\,\sigma = 10^o$.

Discussion. For the specular component, the so called facet model is used. The facet model is the incoherent field based on the Kirchhoff method in the limit of very rough surfaces [1]. For very rough surfaces the coherent component is very low such that the incoherent component describes the total field in this case.

From the theoretical basis of the model we may claim that the model is only valid for very rough surfaces. However, although the model does not give a correct physical description of the scattering mechanisms, it may still represent a reasonable parametric description of the scattering. The model does not account for the scattering platau that may occur at low grazing angles. This can easily be remedied by substituting one of the modified Lambert's rules for the original.

The backscattering strength for the Ellis model is shown in figure 3.1.

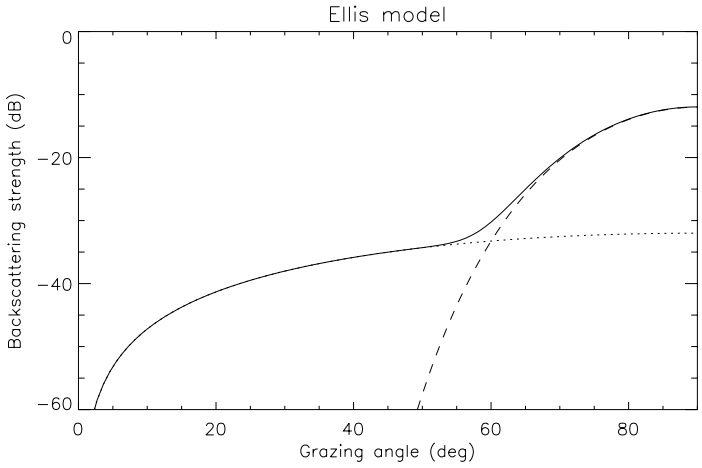

Figure 3.1: Ellis model with μ=-32 dB and ν=-12 dB. The dotted line shows the contribution from Lamberts law, and the dashed line shows the contribution from the facet model.

3.2 The Rough facet model

The Rough Facet Model (RFM) [12, 13, 14] gives an improved expression for the specular scattering component, taking into account not only the loss due to microroughness, but the effects of fine scale roughess as well.

The RFM assumes a surface with two scales of roughness: microroughness and fine scale roughness. By fine scale we mean roughness at scales below the deterministic bathymetry but larger than the acoustic wavelength. By microroughness we mean sub wavelength roughness scales. Determining the partition wavenumbers of the two-scale surface is not trivial, a discussion is given in [13].

The specular term in the RFM has the form [14]

$$\sigma_{coh} = \left[e^{-g_\mu}\right] \left[|R_0|^2\right] \left[\frac{1}{8\pi\gamma^2 \sin^2\theta} \exp\left(-\frac{\cot^2\theta}{2\gamma^2}\right)\right] \tag{3.3}$$

where R_0 is the Rayleigh reflection coefficient (the pressure reflection coefficient for smooth surface), γ is the rms slope of the fine scale facets and g_μ is the roughness parameter for the micro roughness, given by

$$g_\mu = 4\sigma_\mu^2 k^2 \sin^2\theta. \tag{3.4}$$

Here σ_μ is the standard deviation of the micro roughness and k is the acoustic wave number in water.

The rationale for the form of this expression seems to be the following: The last two terms is exactly the incoherent field of the Kirchhoff approximation in the high frequency limit. A interpretation of the expression is that only the specular facets on a surface contributes to the scattered field in any direction. The first term accounts for the additional loss due to microroughness for each (otherwise flat) facet.

The RFM model gives only the coherent component of the scattering, i.e. replaces the second term of eq. 3.2. In eq. 3.3 the effect of microroughness is only to give a loss in the specular direction. But micro roughness also scatters energy in all directions, and its contribution to the total scattering coefficient must also be accounted for, for example by combining the RFM model with the Lambert's rule for diffuse scattering.

3.3 Models based on specular Reflection coefficient

There exists several models for reflection loss. That is, the ratio of specularly reflected to incident acoustic wave at the bottom: The NUC model [15] gives bottom reflection coefficient calculated from porosity (0-1). The MGS [15] and FNWC [15] models calculate the bottom reflection coefficient from bottom province (1-9). All these models are frequency dependent. To this list we may add the Rayleigh bottom reflection coefficient, that is, the plane

wave reflection coefficient at a plane fluid-fluid interface. The Rayleigh model is frequency independent.

The reflection coefficient provided by the NUC, MGS and FNWC models gives the total loss due to both transmission into the bottom and scattering by the surface roughness. The part of the energy scattered away from specular direction by surface roughness, and possibly volume inhomogeneities, constitutes the diffuse scattering component. If we could obtain an estimate of the total amount of scattered energy (into the water), then a scatter law could be constructed by assuming the diffuse component obeys a certain angular distribution, such as the Lambert's rule. In the case of slightly rough surfaces the specular lobe reflects the incident beam width. This approach is along the same lines as suggested by Christol in [16].

4 CONTRIBUTIONS FROM SEDIMENT INHOMOGENEITIES

For some bottom types the contribution from scattering within the sediment can not be neglected compared to roughness scattering. As we have seen above, the volume scattering may dominate at low grazing angles, and for soft sediments, the volume scattering may even dominate for all angles.

Bottom scattering models of varying complexity have been developed. We search a model with few parameters. One such model is described by Novarini [14]. The model uses one free parameter to represent all scattering mechanisms within the sediment.

A major component that is missing from the model is the relationship between the properties of the sediment and the volume scattering "free" parameter of the model. Models are available that connects the volume scattering strength to specific scattering mechanisms, such as [17] and [18]. However, these models require more parameters (at least three), and the parameters that are required by these models (the power spectrum of velocity and density fluctuations in the sediment) are not easy to obtain with the required spatial resolution.

The model of Novarini assumes uniform distribution of scatterers inside the volume and also takes account of the rough boundary. Weak, single and isotropic scattering is assumed. There is one free parameter in the model: the scattering cross section per unit volume m_0. The volume contribution to bottom backscattering is

$$\sigma_v = \mu_v \, V(\theta_i - \alpha_{f0}) \tag{4.1}$$

where

$$V(\theta_i - \alpha_{f0}) = \frac{\cos^4(\theta_i - \alpha_{f0})[1 - \sin^2(\theta_i - \alpha_{f0})/n^2]^{1/2}(m + \sqrt{n^2})^4}{\{m\cos(\theta_i - \alpha_{f0}) + [n^2 - \sin^2(\theta_i - \alpha_{f0})]^{1/2}\}^4} \tag{4.2}$$

and

$$\mu_v = \frac{8m^2 m_0}{\beta \cos\alpha_{f0}[m + \sqrt{n^2}]^4}. \tag{4.3}$$

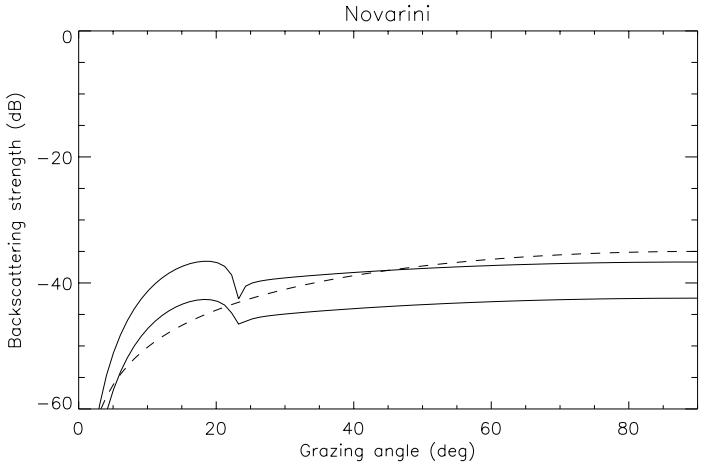

Figure 4.1: Volume scattering due to Novarinis model. The sediment is silt with parameters c=1545 m/s, c_b=1680 m/s, ρ_b=1600 kg/m^3, $m_0 = 4.3 \times 10^{-6}$, α_{f0}=0 and f=1.2 kHz (dataset hnby92_SA in [14]). Backscattering is shown for two values of attenuation: K_p=0.04 dB/m/kHz (upper solid line) and 0.15 $dB/m/kHz$ (lower solid line). The corresponding values for μ_v are -36 and -42 dB respectively. A hump occurs near the critical angle. The dashed line shows the contribution from Lamberts law with μ=-35 dB.

Note that the formulas are given in terms of the incidence angle $\theta_i = 90^0 - \theta$. The angle α_{f0} is the rms slope angle of the surface. The term μ_v is a surface scattering constant attributed to volume scattering, while the angular dependence is given by V.

The sediment is considered to be a lossy medium. Attenuation is introduced by allowing the sound velocity in the sediment to be complex, hence the index of refraction n is

$$n = \frac{c}{c_b}(1 + i\delta_b) \quad \text{and} \quad m = \frac{\rho_b}{\rho} \tag{4.4}$$

where δ_b is a loss parameter given by

$$\delta_b = \frac{K_p\, c_b\, ln10}{40\pi} \tag{4.5}$$

and K_p is the attenuation factor for compressional waves. It has the units $dB/m/Hz$[1]. Further, $\beta = 2kn\delta$ where k is wavenumber, and ρ_b and c_b are the density and sound velocity of the bottom respectively.

Figure 4.1 shows the contribution to backscattering from volume inhomogeneities due to Novarinis model.

The model is demonstrated to perform well for both slow and fast sediments over the frequency range 0.4 to 5 kHz, showing a definite improvement over Lambert's rule.

[1] K_p should have the units $dB/m/Hz$ and not $dB/m/kHz$ as claimed in [14]. $K_p\,(dB/m/Hz) = K_p\,(dB/m/kHz)/1000$.

5 EMPIRICAL BACKSCATTER MODELS

5.1 McKinney and Anderson

The empirical backscatter model of McKinney and Anderson is used in the SEARAY model of ARL, University of Texas. The model computes backscattering as a function of bottom type and frequency.

The basis for the model is the measurements reported in [19]: Measurements of backscatter strength as a function of grazing angle taken over the frequency range 12.5 to 290 kHz in 16 locations around the coast of the US.

For $0 < \theta < 40^0$

$$\begin{aligned}\sigma_b(\theta) &= 1.196\left[(\sin\theta + 0.19)^{B(\cos\theta)^{16}}\right. \\ &\quad \left.\times(2.53F^{(3.2-0.8B)}10^{(2.8B-12)}) + 3.162278\,10^{-5}\right] \end{aligned} \tag{5.1}$$

and for $40^0 < \theta < 90^0$

$$\begin{aligned}\sigma_b(\theta) &= 1.196\left[(\sin\theta + 0.19)^{B(\cos\theta)^{16}}\right. \\ &\quad \times(1 + 125e^{(-2.64(B-1.75)^2 - 50/(\tan^2\theta B))}) \\ &\quad \left.\times(2.53F^{(3.2-0.8B)}10^{(2.8B-12)}) + 3.162278\,10^{-5}\right] \end{aligned} \tag{5.2}$$

Here B is bottom type: $(1 = mud, 2 = sand, 3 = gravel, 4 = rock)$, F is frequency in kHz and θ is grazing angle.

The model is obtained by fitting curves to data, and can therefore not be assumed to be valid outside the frequency range of the data. Due to this restriction the model should not be applied for LFAS frequencies.

Figure 5.1 shows backscattering strength for the McKinney and Anderson empirical model as a function of bottom type.

5.2 TMS models

An empirical model for backscatter index used by Thomson Marconi Sonar (TMS) has the generic form [20]

$$\mu = 0.84 f_{kHz} 10^{-\alpha} \tag{5.3}$$

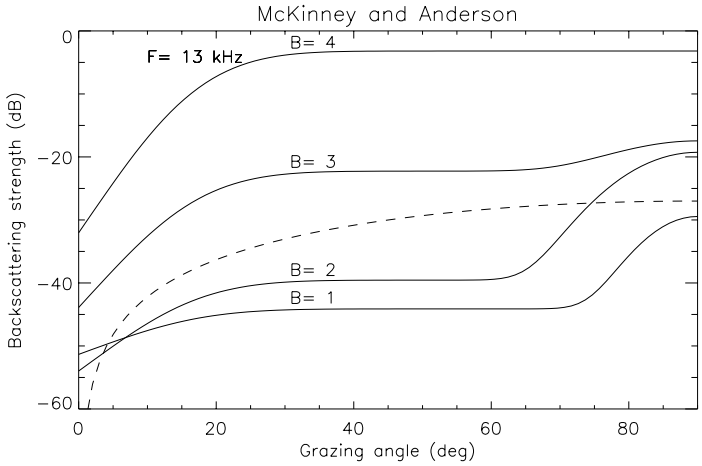

Figure 5.1: McKinney and Anderson empirical model for different values of bottom type, B, and a frequency of 13 kHz. The dashed line shows Lamberts rule with $\mu = -27$ dB.

where f_{kHz} is frequency in kHz and

$$\alpha = 0.1(a + b \cdot Porosity) \tag{5.4}$$

and the Porosity is given in $\%$. The model is simply Lambert's rule with a bottom type and frequency dependent Lambert constant μ. The angle dependence should be explicitly provided. The model is assumed to be valid over the frequency range 1-10 kHz.

Values of α for some sediment types are given in table 5.1. For rock the backscatter index is frequency independent.

Sediment type	α
Sand	3.1
Mud	3.7
Rock	1.8

Table 5.1: TMS empirical model

6 PHYSICAL MODELS

6.1 A perturbation model for roughness scattering

Essen [6] describes a simple first-order perturbation method for scattering from a rough seafloor. The seafloor parameters involved are the roughness spectrum of the the seafloor, and the sound velocities and densities of the water and sediment.

The bottom backscattering cross section is given by

$$\sigma_b = 4k^4 \sin^4\theta \left|R^{(1)}\right|^2 F(2k\cos\theta) \tag{6.1}$$

where k is the total acoustic wavenumber in water, F is the surface roughness spectrum and $R^{(1)}$ is given by

$$|R^{(1)}|^2 = \frac{\left[r^2(2k_h^2 + \gamma_{w0}^2) - 2rk_h^2 - \gamma_{b0}^2\right]^2}{\left(r\gamma_{w0} + \gamma_{b0}\right)^4}. \tag{6.2}$$

Here γ_{w0} and γ_{b0} are the vertical wavenumbers in the water and bottom respectively

$$\gamma_{w0} = \sqrt{k^2 - k_h^2}, \quad \gamma_{b0} = \sqrt{k_b^2 - k_h^2}, \tag{6.3}$$

$k_b = \omega/c_b$ is the total acoustic wavenumber in the bottom, $k_h = k\cos\theta$ is the horizontal wavenumber, and r is relative density, $r = \rho_b/\rho$. The sound velocity and density in the water and bottom are denoted by c, ρ and c_b, ρ_b respectively, see figure 6.1.

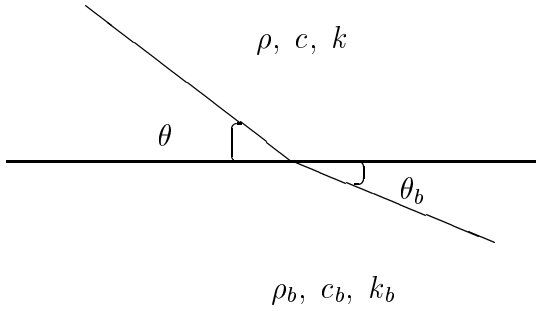

Figure 6.1: Definitions of variables. The quantities for water is unmarked, while the quantities for the bottom are denoted by subscript b. θ is incident grazing angle in water, θ_b is angle of refracted wave. k is total wavenumber in water, k_b is total wavenumber in water. ρ, c are density and sound velocity for water while ρ_b, c_b are density and sound velocity for the bottom.

For the roughness spectrum a power law, or fractal, spectrum is usually assumed:

$$F(k) = \frac{1}{2\pi k} G_0\, k^{-n} \tag{6.4}$$

where G_0 is the spectral strength and n the spectral exponent. Typical values for the spectral exponent are $2 < n < 4$. The spectral exponent affects the frequency dependence of the scattered signal. For $n = 3$ the backscattering becomes independent of frequency. The power law spectrum causes a singularity in the specular direction which limits the valid range of the model. For e.g. a Gaussian roughness spectrum this restriction disappears. First-order perturbation theory is not energy conserving.

The model described in [6] yields the full three-dimensional scattering strength, and includes the effect of shear.

Figure 6.2 shows backscattering strength for the perturbation model for different bottom classes, while figure 6.3 and 6.4 show the effect of varying the sound velocity and density of the sediment.

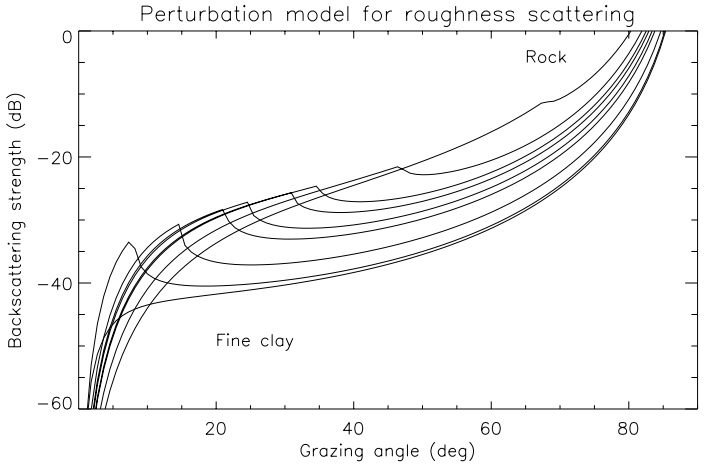

Figure 6.2: First-order perturbation method for roughness scattering. Backscattering strength for predefined bottom classes given in table 6.1. A frequency independent power law roughness spectrum, Eq. (6.4)*, is used with* $G_0 = 0.04$ *and* $n = 3$*. The cusp that is seen in the curves is related to the critical angle.*

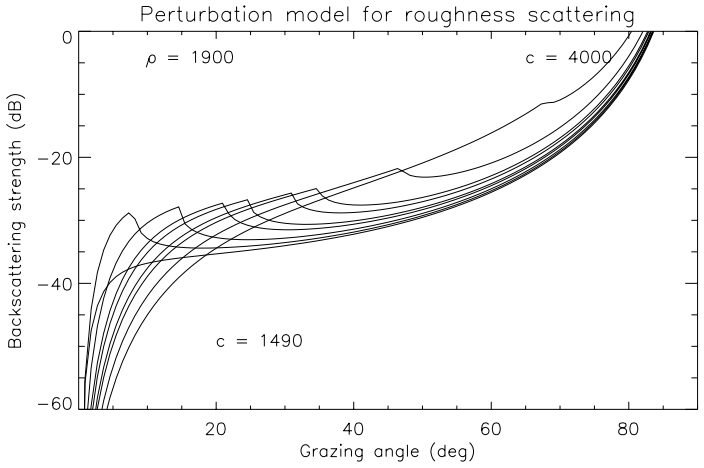

Figure 6.3: Backscattering strength for different values of sound velocity in the range given by table 6.1 and with $\rho = 1900$*. The same roughness spectrum as in figure 6.2.*

Table 6.1: Predefined seafloor classes [21]

Sediment type	$c_p\ (m/s)$	$\rho\ (kg/m^3)$
Water	1500	1000
Rock	4000	2000
Gravel	2200	2000
Coarse sand	1830	2000
Fine sand	1750	1900
Silty sand	1650	1800
Silt	1610	1700
Silty clay	1550	1500
Clay	1515	1400
Fine clay	1490	1400

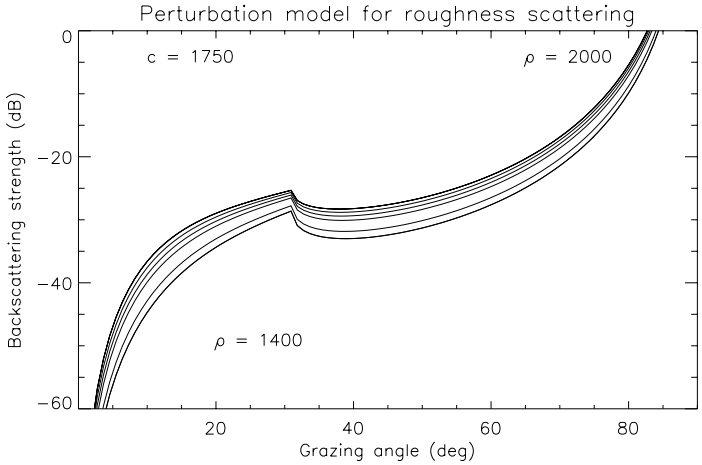

Figure 6.4: Backscattering strength for different values of density in the range given by table 6.1 and with $c = 1750$. The same roughness spectrum as in figure 6.2.

6.2 A perturbation model for volume scattering

Yamamoto [18] has developed a first order perturbation model for scattering from a sediment volume. The model is based on the Born approximation and the Wood sediment model, and computes the wave field scattered from the velocity and density fluctuations within the sediment.

The model includes the effects of propagation to the scattering volume and back to the receiver as well as attenuation in the sediment.

The differential backscattering cross section per unit surface of the seabed is

$$\sigma_a = \sigma_v \left(\frac{\sin\theta_b}{4\alpha} \right) T_{12}^2 T_{21}^2 \left(\frac{\cos^2\theta_b}{\cos^2\theta} \frac{\sin^2\theta}{\sin^2\theta_b} \right) \tag{6.5}$$

where σ_v is the scattered differential cross section per unit volume

$$\sigma_v = 2\pi k_{b0}^4 (1+2\gamma)^2 S_\mu(-2k\mathbf{e}_i) \tag{6.6}$$

and T_{12} and T_{21} are the transmission coefficients given by

$$T_{12} = \frac{2\rho_b c_b \sin\theta}{\rho_b c_b \sin\theta + \rho c \sin\theta_b} \tag{6.7}$$

$$T_{21} = \frac{2\rho c \sin\theta_b}{\rho c \sin\theta_b + \rho_b c_b \sin\theta} \tag{6.8}$$

Fluctuations of sound speed and density in the sediment are defined by

$$c_b = c_{b0}(1+\mu) \tag{6.9}$$

$$\rho_b = \rho_{b0}(1+\eta) \tag{6.10}$$

where ρ_{b0}, c_{b0} are the background density and sound velocity in the sediment. The quantity γ is the ratio of relative density to velocity fluctuations in the sediment, $\gamma = 2\eta/\mu$. S_μ is the spectrum of the relative velocity fluctuations in the sediment, k_{b0} is the background wavenumber in the sediment defined by $k_{b0} = \omega/c_{b0}$, further ρ, c are the density and sound velocity in water and $\mathbf{e}_i$ is a unit vector in the direction of the incident plane wave.

For the spectrum of velocity fluctuations Yamamoto suggests a power law spectra given by

$$S_\mu(k_1,k_2,k_3) = \frac{\beta\Lambda^2 B}{2\pi}(\Lambda^2 k_1^2 + \Lambda^2 k_2^2 + k_3^2)^{(\beta+2)/2} \tag{6.11}$$

where B is the spectral strength, β is the spectral exponent and Λ describes the anisotropy (horizontal to vertical correlation length) of inhomogeneities in the sediment. Horizontal isotropy is assumed. The wavenumbers in direction x, y and z are given by k_1, k_2 and k_3 respectively.

The model requires the following physical parameters: the sound velocities and densities of the water and sediment, the relative density fluctuation in the sediment, as well as three parameters to describe the spectrum of velocity fluctuations in the sediment: the spectral strength, spectral exponent and vertical anisotropy.

7 CONCLUSIONS

Below we sum up the requirements for a local scatter model, and suggest a few scatter models of increasing complexity.

7.1 The needs

A local scatter model should be provided, for modelling backscatter from a low frequency activated towed sonar (CAPTAS).

For this purpose we require a backscatter (not bistatic) model which is valid for low to moderate grazing angles and slightly rough surfaces. The model should include the effects of both roughness and volume scattering.

The difficult question of defining the border between roughness and topography will not be raised here. We claim that for the low frequencies to be used during the CAPTAS measurements, the bottom can be safely considered to be slightly rough, and that, for the experiments, high resolution topography will be available to account for the larger scale irregularities.

The contribution to backscattering from the sediment volume is expected to be small for hard/fast sediments, but can be significant, or even dominate for slow, soft sediments. The sediment types we expect in the measurement area ranges from soft (clay) to relatively hard (sand, gravel) such that volume scattering can not be ruled out.

7.2 Limitations of the measurement and consequences for scatter model

The proposed measurements will provide backscatter data over a relatively small angular span at low grazing angles since, at long ranges, the rays hitting a bottom facet is confined to a narrow sector close to grazing incidence. Fitting a scattering model with many parameters to measurements over a very limited angular range will probably not give stable and consistent results. The frequency dependence of scattering may be utilized to provide additional information, as well as information from steeper incidence angles provided by the short range measurements.

7.3 A simple empirical model

If the specular component is of no concern, which is the case for backscattering at low grazing angles, the model of Del Balzo seems like a good choice. The model depends on one parameter. An alternative is the Lambert's rule with a threshold, which depends on three parameters.

7.4 A simple physical model

For roughness scattering we suggest to use the the first-order perturbation model of section 6.1. To complement this model we suggest the volume scattering model of Yamamoto [18], described in section 6.2. For 2-D calculations these models require eight physical parameters.

APPENDIX

A Collection of Published Information about Roughness and Topography of Sea-Beds

I. ROUGHNESS FEATURES

Bottom photograph at 30°14'N 78°07'W (Blake Plateau)

(from Medwin & Clay, p.357)

D.R.Jackson & K.B.Briggs *"High-frequency bottom backscattering: roughness versus sediment volume scattering"*, *in* **J.Acoust.Soc.Am. 92(2, Pt.1)**, pp.962-977 (1989)

Analysis techniques: > box coring (6.1 cm diameter cores) → geoacoustic properties
> Stereophotography (twin 70-mm underwater cameras) & photogrammetric stereocomparator → roughness

"Quinault" Site: 47°34'N, 124°35'W
North Pacific, 17.km west of the coast of the State of Washington
Fine sand bottom with pronounced directional (N.NW-to-S.SE) non-very-steep ripples, probably remaining from winter storms, several months before. Low biological activity?
Little vertical variations of sediments over the 29 first cm.

Arafura Sea: 10°01'S, 137°50'E
Indian Ocean. 255 km north-north-west of Cape Arnhem, Australia)
Relatively smooth bottom. Bimodal distribution of sizes: silty-clay matrix, bearing numerous buried shell fragments, sand and gravels (55% of weight), etc. Quite strong variatbility of sediment properties over the 35 first cm.
No significant anisotropy for the roughness.

"San Francisco" Site38°39'N, 123°29'W
Pacific. 180 km northwest of San Francisco
Moderately rough silty bottom. Steep variations of porosity and attenuation-rate over the 7 first cm, probably due to "bioturbation" (activity of burrowing or buried animals); deeper sediments are more uniform.
Urchins and starfishes are abundant, and visible at sediment-water interface. Mean densities: daytime, 1.6 living urchins per m^2; (night: 2.8 & 8.7); up to 25 per m^2. Daytime: 3.3 living starfishes per m^2 (night: 1.0 & 8.9); up to 22. These animals form herds, and are essentially nocturnal; they bury themselves during daytime, with two effects on superficial sediments: they increase the porosity of the first cm's, and they make isotropic the bottom roughness (well oriented crests from storms and currents are erased)..
Ripples: before storm, low-relief, uniform, isotropic bottom, featuring mounds and holes (animals). After storm, well-defined clearly N-NE to S-SW oriented crests (Roughness height: 1.9 cm).

1) **Sediment Parameters**

Site	Depth (m)	Bottom nature	Porosity (%)	Grain size (ϕ)	Sound-speed ratio	Density ratio	Attenuation (dB m^{-1} kHz^{-1})
Quinault	49.	Fine sand	41.2 ± 2.1 *40.5 ± 1.2*	2.94 ± 0.11 *2.97 ± 0.06*	1.113 ± 0.013 *1.113 ± 0.009*	1.93 ± 0.03 *1.94 ± 0.02*	0.37 ± 0.12 *0.30 ± 0.04*
Arafura	47.	Sand-silt-clay & Clayey sand	69.7 ± 4.0 *77.8 ± 5.2*	5.24 ± 0.78 *5.63 ± 1.11*	0.986 ± 0.004 *0.988 ± 0.005*	1.49 ± 0.07 *1.39 ± 0.09*	0.84 ± 0.29 *0.20 ± 0.09*
San Francisco	90.	Silt	63.4 ± 3.9 *72.8 ± 2.0*	6.35 ± 0.45 *6.39 ± 0.29*	1.009 ± 0.005 *1.002 ± 0.003*	1.58 ± 0.07 *1.41 ± 0.03*	0.56 ± 0.08 *0.37 ± 0.06*

> in normal characters: values averaged over the full core length (from 10.cm to 39.cm)
> in *Green italics*: values over the surficial first 2 cm of sediments

***2)* Roughness Parameters**

Site	Bottom nature	Bounds of spatial spectrum interval (cycles / cm) lower bound	upper bound	Slope of roughness power-spectrum		Spectrum (cm^3) at 1 cycle /cm	
Quinault	Fine sand	0.033	1.0	* -2.92 ** -2.67		* $2.8\ 10^{-4}$ ** $3.3\ 10^{-4}$	
Arafura	Sand-silt-clay & Clayey sand	0.020	1.8	-2.18		$6.9\ 10^{-4}$	
San Francisco	Silt	0.02	1.1	* **-2.65** ** **-2.38**	* *-2.73* ** *-2.56*	* **$7.2\ 10^{-5}$** ** **$1.3\ 10^{-4}$**	* *$5.7\ 10^{-5}$* ** *$1.27\ 10^{-4}$*

Roughess spectrum:
> * : along strike direction (parallel to main ripple crests)
** : across strike direction (normal to main ripple crests)

San Francisco: *Red italics:* after storm
Blue bold: before storm

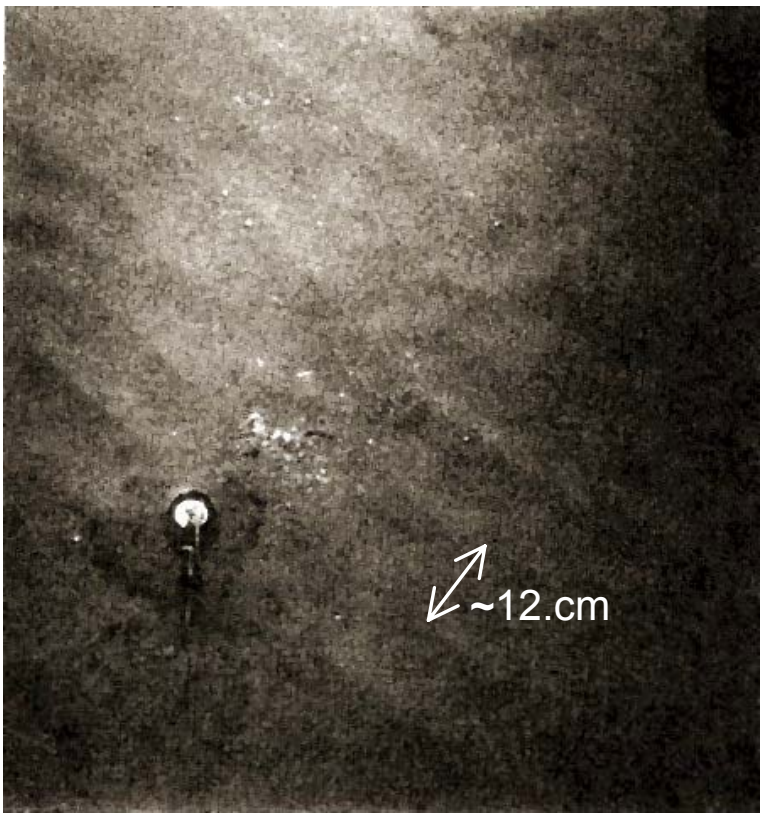

"Quinault" Site

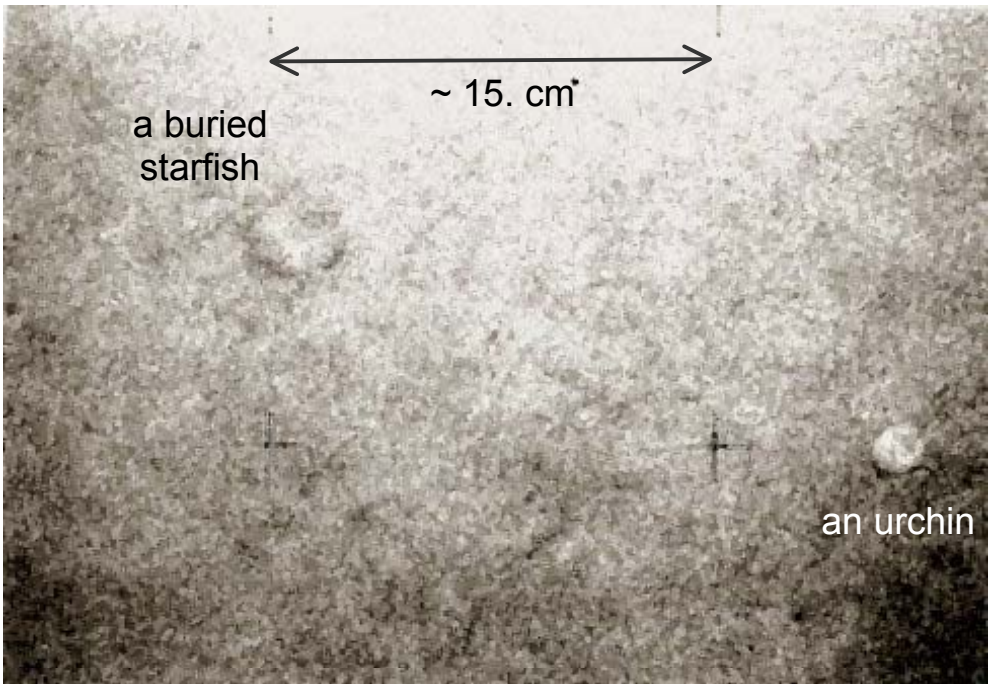

"San Francisco" Site

S.Stanic, K.B.Briggs, P.Fleischer, W.B.Sawyer & R.I.Ray
"High-frequency acoustic scattering from a coarse shell ocean bottom",
in **J.Acoust.Soc.Am. 85(1)**, pp.125-136 (1989)

"Jacksonville" Site:
27 miles east of Jacksonville, Florida (North-west limit of Florida)
Coarse sand and gravel. Two different types of sand: "**light**" sand, coarse, with broken parcels of shells, alternating with coarser "**dark**" sand bearing full shells. The bands of alternating different sands may give the illusion of strong roughness.

Sediment Parameters

Site	Depth (m)	Bottom nature	Porosity (%)	Grain size (ϕ)	Sound-speed ratio	Density ratio	Attenuation (dB m^{-1} at 400 kHz)
Jacksonville	~ 25	Coarse ***"light"*** & ***"Dark"*** shell-sands 5% Gravel	39. (32 to 46)	0.84 (very skewed distribution; lower extension up to -4)	1.113 ± 1.76%	1.993 (2.039 $g.cm^{-3}$)	mean: 583 (249 to 1322)

Roughness Parameters

Site	Bottom nature	R.m.s. roughness height (cm)			Slope of roughness power-spectrum		
		150°	240°	all directions	150°	240°	all directions
Jacksonville	Coarse sand	0.450 0.312 0.387	0.394 0.494 0.447	0.423 0.413 0.418	-1.54 -1.43 -1.50	-1.38 -1.49 -1.44	-1.47 -1.48 -1.47

Roughess spectrum along normal azimuthal directions (150° and 240°), averaged over all 18 analysed directions.

Blue: *site n°103* - Green: *site n°111* - Red: *averaged over all photographed sites*

Window for spectral analysis: about 0.01 cycle/cm - 1.2 cycle/cm - Value at 1 cycle /cm: about $10^{-2}cm^3$

D. R. Jackson, K. B. Briggs, K. L. Williams, & M. D. Richardson
"Tests of Models for High-Frequency Seafloor Backscatter",
in **IEEE Journal of Oceanic Engineering 21(4)**, pp.458-470 (1996)

Eckernförde 54°29.5'N, 9°59,0'E A shallow bay in southwestern Baltic Sea. Shallow depth: 26.m. Silty-clay sediments, with a layer of methane bubbles at 1.m below water (**dominant** phenomenon for back-scattering).
Panama City 29°41.1'N, 85°40.7'W Shallow depth: 29.m. Coarse sand, with coarse shell hash.
Key West 24°36.7'W, 82°50.7' South Florida Islet. Shallow depth: 25.m. Carbonate sand-silt-clay.

Experimental Estimates of Different Bottom Parameters

Site	Grain size (ϕ)	Velocity rate	Attenuation ($dBm^{-1}kHz^{-1}$)	Porosity (%)	Density Ratio	Shear velocity (m/s)
Eckernförde	9.9	0.991	0.0707	86.0	1.18	8.1
Panama	0.8	1.126	0.524	40.1	1.97	117.
Key West	6.5	1.020	0.321	56.4	1.72	56.4

Site	Velocity ratio		Porosity		Roughness spectrum	
	variance (m^2/s^2)	Vertical corr. length (cm)	variance ($\%^2$)	Vertical corr. length (cm)	slope	value at 1 cycle/cm (cm^3)
Eckernförde	3.62	4.63	0.617	2.11	-2.42	$3.028\ 10^{-4}$
Panama	406.45	1.37	3.90	1.06	-2.12	$1.983\ 10^{-3}$
Key West	38.72	4.65	7.25	2.81	-2.29	$2.092\ 10^{-3}$

K. B. Briggs *"Microtopographical Roughness of Shallow-Water Continental Shelves"*, *in* **IEEE Journal of Oceanic Engineering 14(4)**, pp.360-367 (1989)

Site Name	Bottom nature	Depth (m)	R.m.s. roughness height (cm)	Roughness spectrum Slope	Value at 1.cycle/cm (cm^3)	
> Anisotropic Roughness Field						
Mission Bay 1, Califonia	Coarse Sand	18.	2.30	-2.46 ---	$5.7\ 10^{-4}$ ---	normal to crests along crests
Quinault, Washington	Fine Sand	49.	1.76	-2.67 -2.92	$3.3\ 10^{-4}$ $2.8\ 10^{-4}$	normal to crests along crests
Charleston 1, South-Carolina	Medium Sand	20.	0.37	-2.29 -1.33	$0.8\ 10^{-4}$ $5.4\ 10^{-4}$	normal to crests along crests
> Isotropic Roughness Field						*Pathlength (cm)* / *Sampling step (cm)*
Mission Bay 2, Califonia	Fine Sand	18.	0.93	-2.17	$1.23\ 10^{-3}$	*161.9* / *0.635*
Montauk, New York	Fine Sand	35.	0.28	-2.72	$3.\ 10^{-5}$	*127.5* / *0.5*
Charleston 2, South-Carolina	Fine Sand	21.	0.39	-2.50	$9.\ 10^{-5}$	*31.5* / *0.5*
Arafura Sea West Australia	Mud	50.	0.37	-2.18	$6.9\ 10^{-4}$	*35.6* / *0.28*
Panama City, Panama	Fine Sand	31.	0.49	-1.92	$2.33\ 10^{-3}$	*53.3* / *0.42*
Charleston 3, South-Carolina	Shell Hash	20.	0.29	-2.05	$8.\ 10^{-5}$	*31.5* / *0.5*
Jacksonville, Florida	Shell Hash	27.	0.42	-1.47	$5.34\ 10^{-4}$	*53.3* / *0.42*

Pouliquen-Lurton Synthetic Classification along Mean Bottom Properties for Inversion from Acoustic Reverberation

		Sedimentary Bottoms							
Original Table of Pouliquen & Lurton, *in* Acta Acustica 2 (1994), p.117	**Bottom Index**	**1**	**2**	**3**	**4**	**5**	**6**	**7**	
	Bottom Type	*Soft Mud*	*Mud*	*Sand-Mud*	*Fine Sand*	*Sand*	*Gravel*	*Rock*	
	Potential Sound-Speed c (m/s)	1520.	1520.	1600.	1650.	1750.	2200.	4000.	
	Density ρ ($g.cm^{-3}$)	1.5	1.5	1.7	1.75	1.95	2.0	2.6	
	Attenuation coefficient β (dB/λ)	0.15	0.15	0.20	0.20	0.80	0.50	0.10	
	R.m.s. roughness slope δ (°)	**3.**	**4.**	**3.**	**4.**	**6.**	**7.**	**11.**	**The most innovative set of data**
	Stand. dev. of volumic variability μ (%)	**5.**	**3.**	**2.**	**<1.**	**3.**	**<1.**	**<1.**	
Other bottom features	**Mean Grain Size*** (ϕ)	10 - 8	7 - 6	5 - 4	3 - 2	1 - 0	< 0	*not sedimentary*	
	Porosity* (%)	80-75	75-60	60-50	50-40	40-35	40-35	35 - 0 *(solid rough layer)*	

* freely extrapolated with the help of **Hamilton**'s data

E. Pouliquen & X. Lurton

"Identification de la nature du fond de la mer à l'aide de signaux d'écho-sondeurs:"
" I. Modélisation d'échos réverbérés par le fond",
in **Acta Acustica 2**, pp.113-126 (April 1994)
"II. Méthode d'identification et résultats expérimentaux",
in **Acta Acustica 2**, pp.187-194 (June 1994)

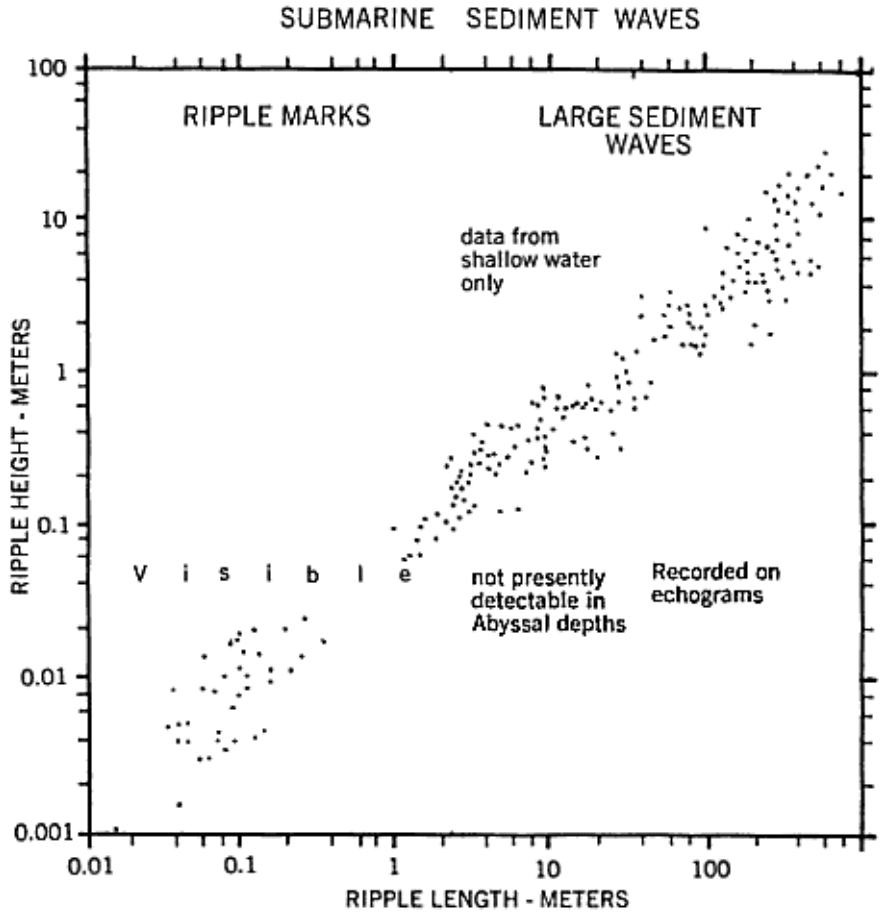

(from B.C.Heezen & Ch.D.Hollister, ***THE FACE OF THE DEEP***, Oxford University Press, 1971)

II. TOPOGRAPHICAL FEATURES

J. M. Berkson, & J. E. Matthews *"Statistical Properties of Sea-Floor Roughness"*, *in* **N. G. Pace, ed.** *ACOUSTICS AND THE SEA-BED*, *Bath University Press, UK* (1983), pp.215-223

A TABLE OF STATISTICS FOR SEABED TOPOGRAPHY

Physiological Province	**Ocean**	**Band-Limited* R.m.s. Roughness Height (m)**	**Roughness Spectral Slope**
Continental Rise	Atlantic Ocean	3.7	3.2
Continental Slope	Atlantic Ocean	6.4	2.2
Seamount	Atlantic Ocean	3.6	2.1
Abyssal Plain	Atlantic Ocean	< 1.3	-
Abyssal Plain	Atlantic Ocean	< 1.5	-
Continental Rise	Norwegian Sea	< 1.1	-
Abyssal Hills	Pacific Ocean	3.4	4.9
Continental Shelf	Norwegian Sea	2.5	2.0
Marginal Plateau	Norwegian Sea	1.9	1.9
Abyssal Hills	Pacific Ocean	2.5	4.2
Continental Rise	Mediterranean Sea	< 1.4	-
Continental Rise	Norwegian Sea	< 1.2	-
Marginal Plateau	Norwegian Sea	2.1	1.5
Abyssal Hills	Pacific Ocean	2.3	2.2
Continental Rise	Mediterranean Sea	< 1.0	-
Basin	Norwegian Sea	5.4	1.8
Sediment/Basalt Interface	*Atlantic Ocean*	*258 ± 54*	*1.8 ± 4*
Sediment/Basalt Interface	*Pacific Ocean*	*99 ±36*	*1.8 ± 4*

* Spatial wave-number band: 3.10^{-3} m^{-1}- 3.10^{-2} m^{-1}
(Wave-length: 200.m-2.km)

except for *Basaltic interfaces:* 6.10^{-5} m^{-1}- 3.10^{-3} m^{-1}
(Wave-length: 100.km-2.km)

C..Clay & W.K.Leong *"Acoustic estimates of the topography and roughness spectrum at the seafloor southwest of the Iberian Peninsula"*
in **L. Hampton, ed.** ***Physics of Sound in Sediments***, Plenum Press, New York (1974)

Index of Region	Roughness over bounded interval			
	interval I (cm)	*interval II* (m)	*interval III* (m)	*interval IV* (m)
1	2.9 ± 0.3	0	0	0
2	X	X	191. ± 20.	293. ± 31.
3	2.4 ± 0.3	0	1.7 ± 0.2	1.1 ± 0.1
4	X	X	81. ± 9.	236. ± 25.
5	0	0	100. ± 11.	236. ± 25.
6	X	X	14.6 ± 1.6	690. ± 74.
7	2.3 ± 0.3	0	100. ± 11.	191. ± 20.
8	X	X	100. ± 11.	363. ± 39.
9	2.9 ± 0.3	2.6 ± 2.8	5.0 ± 0.5	293. ± 31.
10	X	X	293. ± 31.	690. ± 74.
11	2.4 ± 0.3	4.0 ± 0.4	5.0 ± 0.5	0
12	2.4 ± 0.3	3.3 ± 0.4	18. ± 2.	363. ± 39.
13	X	X	18. ± 2.	363. ± 39.
14	X	X	22. ± 2.	1313. ± 141.
15	X	X	124. ± 13.	2015. ± 216.
16	1.9 ± 0.2	4.0 ± 0.4	81. ± 9.	0.
17	11. ± 1.	1.7 ± 0.2	1.7 ± 0.2	0
18	2.4 ± 0.3	0	0	0
19	2.9 ± 0.3	0	18. ± 2.	1312. ±141.
20	2.9 ± 0.3	0	100. ± 11.	1060. ±141.
21	2.4 ± 0.3	2.6 ± 0.3	100. ± 11.	1312. ±141.
22	0.3 ± 0.3	0	100. ± 11.	0
23	0.4 ± 0.4	3.3 ± 0.3	154. ± 17.	450. ± 48.
24	2.4 ± 0.3	1.71 ± 0.18	154. ± 17.	293. ± 31.
25	16. ± 2.	5.0 ± 0.5	81. ± 9.	293. ±

				31.
26	X	X	18. ± 2.	363. ± 39.
27	3.6 ± 0.4	3.3 ± 0.3	100. ± 11.	1313. ±141.
28	3.6 ± 0.4	0	28. ± 3.	1313. ±141.
29	3.6 ± 0.4	0	0	0
30	X	X	124. ± 13.	1626. ±175.

Index of Region	Roughness (m) over bounded intervals			
	interval I (cm)	*interval II* (m)	*interval III* (m)	*interval IV* (m)
31	3.6 ± 0.4	3.3 ± 0.3	18. ± 2.	363. ± 39.
32	2.9 ± 0.3	2.6 ± 0.3	5.0 ± 0.5	0
33	0	0	22.5 ± 2.4	0
34	2.9 ± 0.3	0	18. ± 2.	1060. ±114.
35	X	X	293. ± 31.	1060. ±114.
36	X	X	22.4 ± 2.4	1060. ±114.
37	X	X	22.4 ± 2.4	363. ± 39.
38	X	X	363. ± 39.	1060. ±114.
39	2.4 ± 0.3	5.0 ± 0.5	18. ± 2.	236. ± 25.
40	X	X	293. ± 31.	293. ± 31.
41	3.6 ± 0.4	0	18. ± 2.	0
42	3.6 ± 0.4	2.6 ± 0.3	6.2 ± 0.7	124. ± 13.
43	0	0	363. ± 39.	363. ± 39.
44	3.6 ± 0.4	0	0	0
45	4.5 ± 0.5	3.3 ± 0.3	3.3 ± 0.3	0
46	X	X	293. ± 31.	1060. ±114.
47	X	X	22.4 ± 2.4	1313. ±141.
48	13.0 ± 1.4	3.3 ± 0.3	3.3 ± 0.3	557. ± 60.
49	X	X	22.4 ± 2.4	0

50	3.0 ± 0.3	0	100. ± 11.	0
51	3.6 ± 0.4	2.1 ± 0.2	18. ± 2.	0
52	13.0 ± 1.4	5.0 ± 0.5	124. ± 13.	0
53	2.4 ± 0.3	2.1 ± 0.2	81. ± 0.7	293. ± 31.

Error bars refer to an uncertainty of one pixel on the scanned picture, not on the experimental errors, that are not given in the paper.

	Interval in wave-length	
I	$\lambda < 200.\text{m}$	← roughness
II	$200.\text{m} < \lambda < 2.\text{km}$	← micro-topography
III	$2.\text{km} < \lambda < 12.\text{km}$	← relief
IV	$12.\text{km} < \lambda < 200.\text{km}$	← large-scale relief

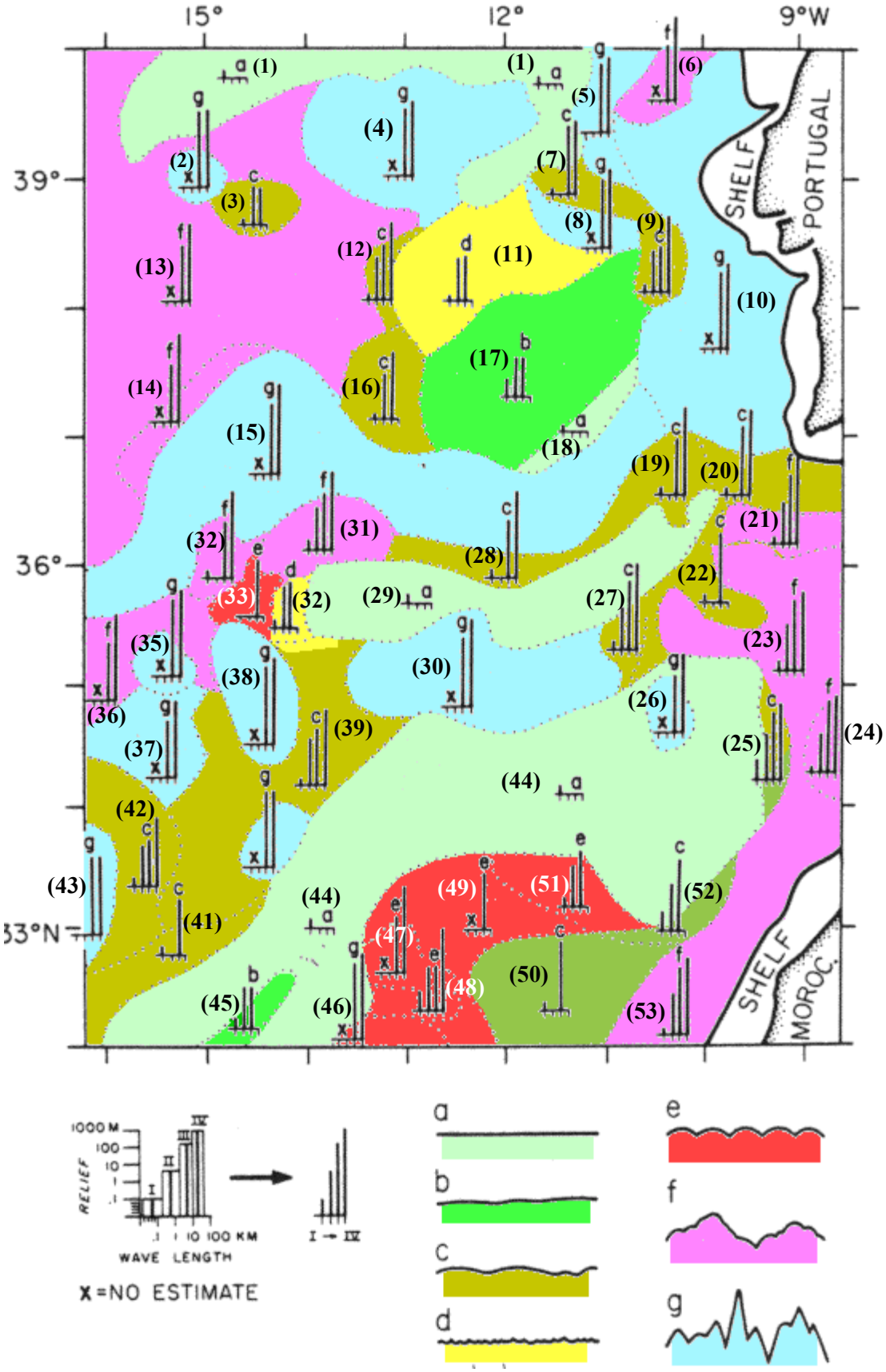
15°
12°
9°W
39°
36°
33°N
SHELF
PORTUGAL
SHELF
MOROC.
1000 M
100
10
1
.1
RELIEF
.1 1 10 100 KM
WAVE LENGTH
I → IV
X=NO ESTIMATE
a
b
c
d
e
f
g

S.Stanic, K.B.Briggs, P.Fleischer, W.B.Sawyer & R.I.Ray
"High-frequency acoustic scattering from a coarse shell ocean bottom",
in **J.Acoust.Soc.Am. 85(1)**, pp.125-136 (1989)

"Jacksonville" Site:
27 miles east of Jacksonville, Florida (North-west limit of Florida)
Coarse sand and gravel. Two different types of sand: "**light**" sand, coarse, with broken parcels of shells, alternating with coarser "**dark**" sand bearing full shells. The bands of alternating different sands may give the illusion of strong roughness.

Micro-topography (Bottom variations of the order of a few m in heigh, with an horizontal resolution of the order of 200.m)

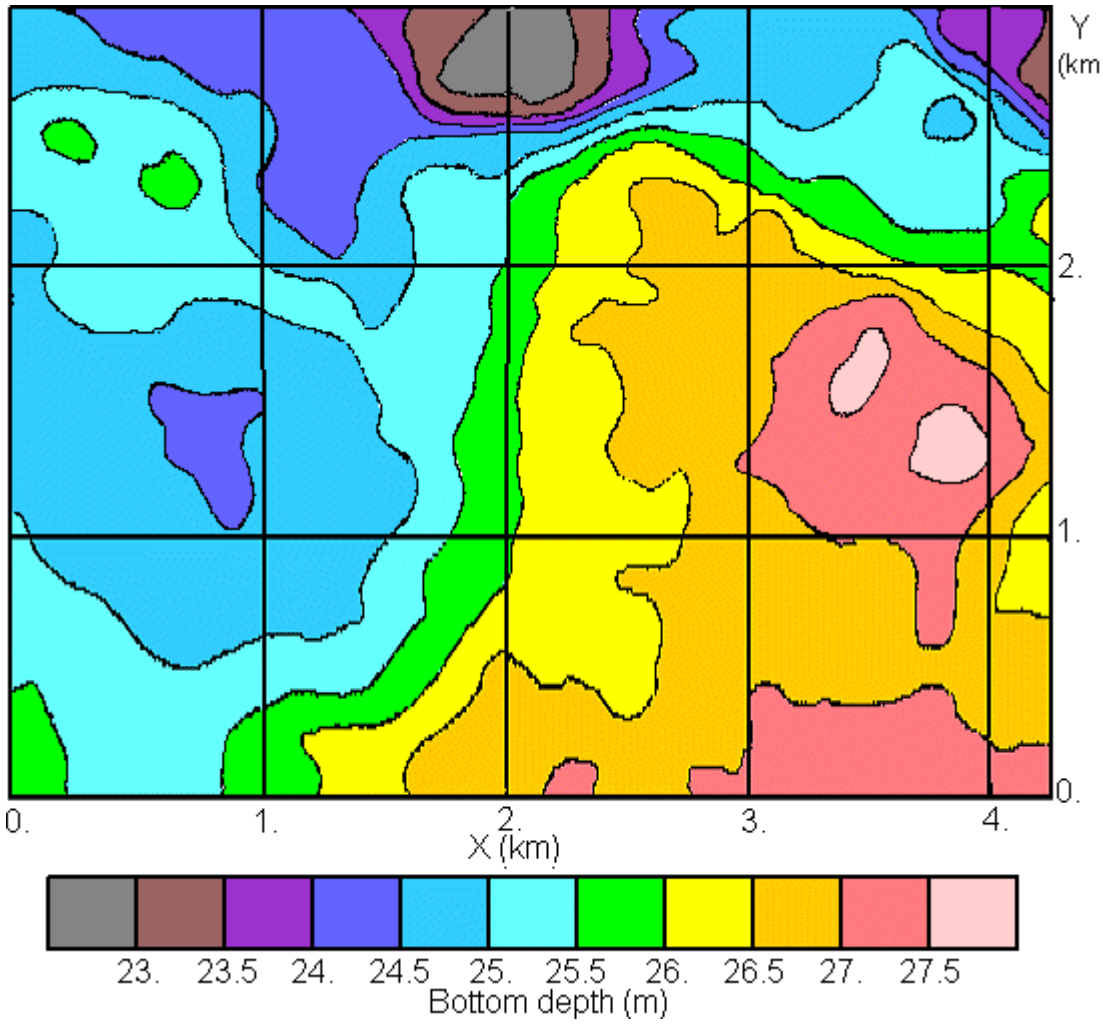

(redrawn and adapted from **Stanic** *et al*., 1989, p.127)

DUNE & SAND-WAVES FIELDS - TIDAL RIDGES

Some information borrowed among others from:

K. R. Dyer ***COASTAL AND ESTUARINE SEDIMENT DYNAMICS***
Wiley & Sond, Chichester, 1986

and: H. Chamley ***LES MILIEUX DE SEDIMENTATION***
BRGM:Lavoisier, Orléans/Paris, 1988

Nomenclature of Bedforms, Empirical Relations & Typical Orders of magnitudes (from Dyer, 1986, pp.129-143, 272-282 and Chamley, 2000, pp.69-78)

Notations: λ = wave length of roughness, or relief - H = height of roughness, or relief
D = grain diameter - $\mathbf{Z_B}$ = water depth - **V** = velocity of roughness or relief advance
u = ambiant fluid velocity - $\mathbf{u_{10}}$ = ambiant fluid velocity at 10.cm over bottom (ripples)
$\mathbf{u_C}$ = threshold friction velocity (minimum velocity for transporting grains):

		→ *increasing sizes* →	
Wave length λ	commonly 20-30 cm $\lambda \sim 1000\ \mathbf{D}$ (up to 18 m observed)	$\lambda \sim 2\pi\ \mathbf{Z_B}$ (unidirectional flow) 0.5m < λ ; commonly 5-10.m	from some 15.m ('major dunes' in tidal zones) up to 600-900.m
Height H	from 2-3 times **D** ("young" ripples) up to a 2-3 cm (common)	H < critical height $\mathbf{Z_B}/6$ (unidirectional flow) H spans from 6.cm to 1.5 m Commonly ~30.cm (tidal areas)	1.5-3.m to 15.-18.m
Steepness & Slope	H/λ < 1/10 ~ 5° (upstream) ~ 32° (downstream)	H/λ < 1/30 (maybe up to 1/17) ~ 5° (upstream)	$H \sim 0.0635\ \lambda^{0.733}$ H/λ commonly 1/10-1/15 < 6°-10° (averages ~1.5°)
Conditions to existence	$1 < \mathbf{u}/\mathbf{u_C} < 3.5$	$1 < \mathbf{u}/\mathbf{u_C} < 8$ (0.6 m/s < u) Coarse (but not too much) grain: 0.6 mm (0.1 mm) < **D** < 8.mm	Maximal tidal velocity > 0.6-1.3 m/s (0.3-0.8m/s) 0.25 mm < **D**
Movements	irregular, may be very fast (image of currents), downstream $\mathbf{V} \sim 2.02\ 10^{-10}\ u_{10}^{5}$	$\mathbf{V} \sim$ 1.m/day	Very wide range of migration rate: from quasi-motionless at geological scales up to **V** around 13 m/year, 35-150 m/yr

Oscillatory tidal flows	**Ripples**	**Mega-ripples**, *alias* **Dunes** *alias* **Small Sand waves**	**Sand waves** *alias* **Large Sand waves**
Unidirectional flows	**Ripples**	**Dunes**	
Remarks	Wavelength λ mainly depends on grain size **D**	Wavelength λ mainly depends on water depth $\mathbf{Z_B}$ Slight dependence on grain size **D**	Carry conventional ripples and dunes on their backs (H~0.5-1.m - λ~5-10m in unidirectional flows)

1/ → Ripples
2/ → Dunes
3/ → Sand-Waves

Later stages in the bedform-sequence (when increasing flow velocity):

4/ → High-Stage Plane Bed (flow too fast for allowing sand waves, but not enough for producing anti-dunes)

5/ → Anti-Dunes (deposition occurs on the upstream side, erosion on downstream side; the anti-dunes move downstream)

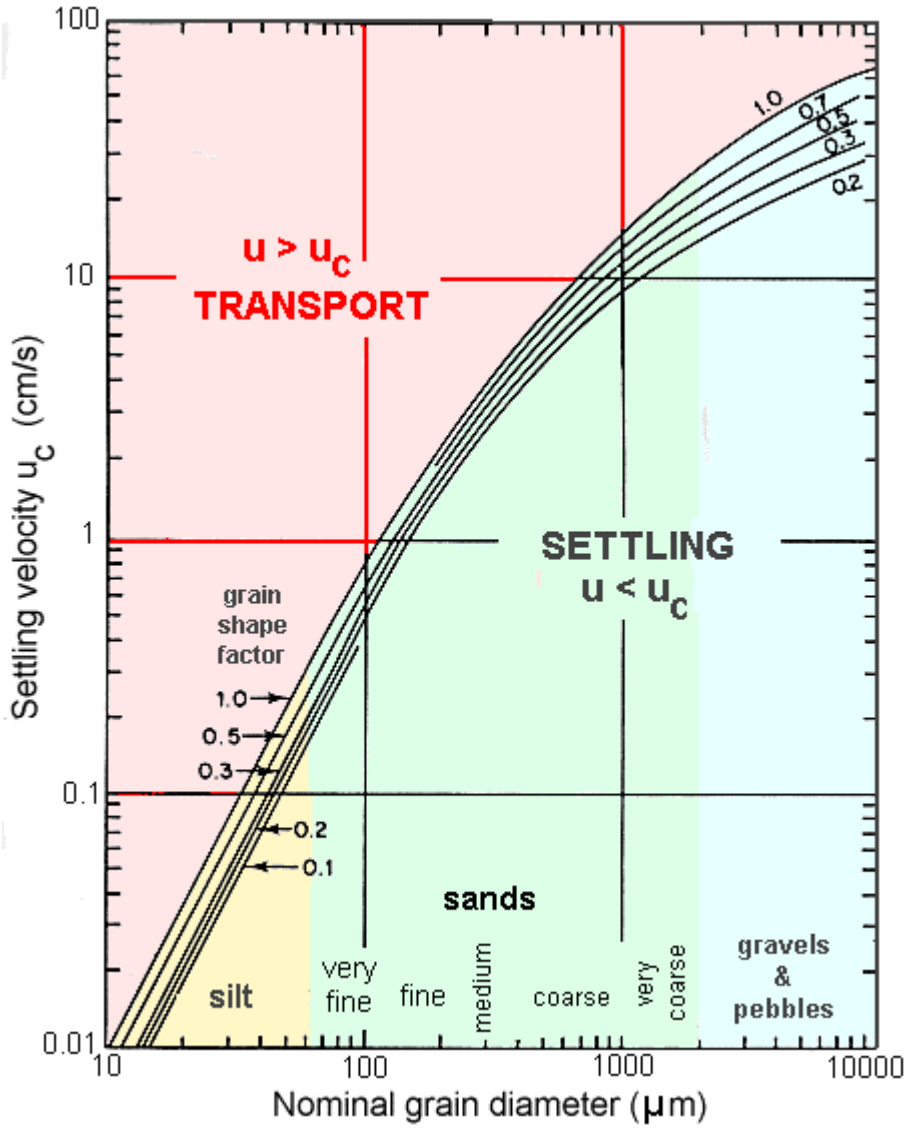

(from Dyer, 1986)

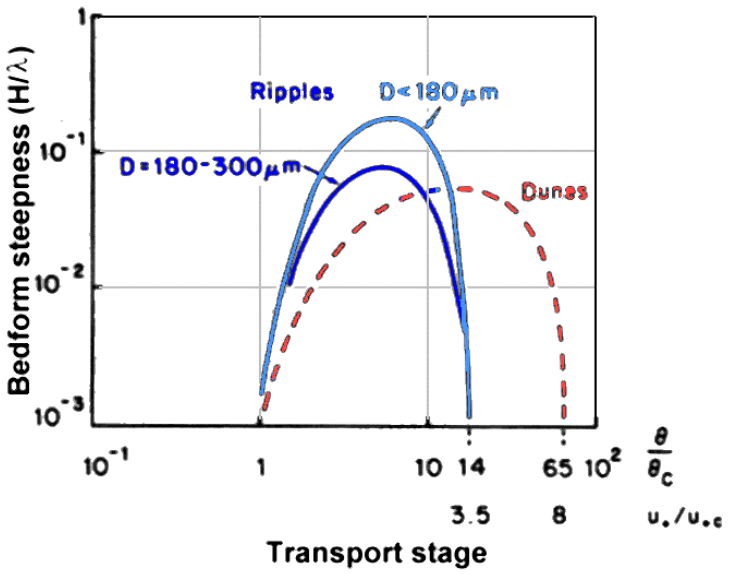

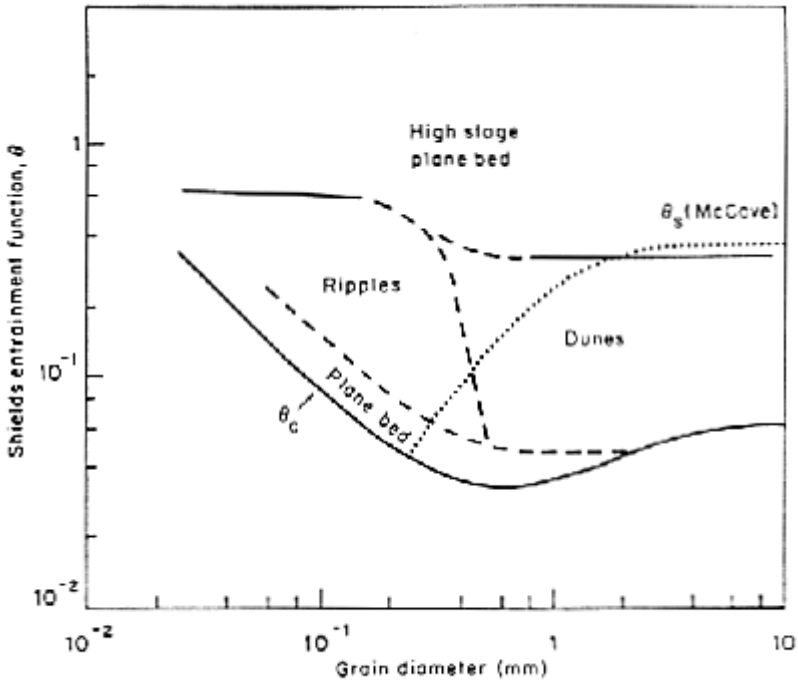

Figure 4.19 Limits of occurrence of bedforms (various authors)

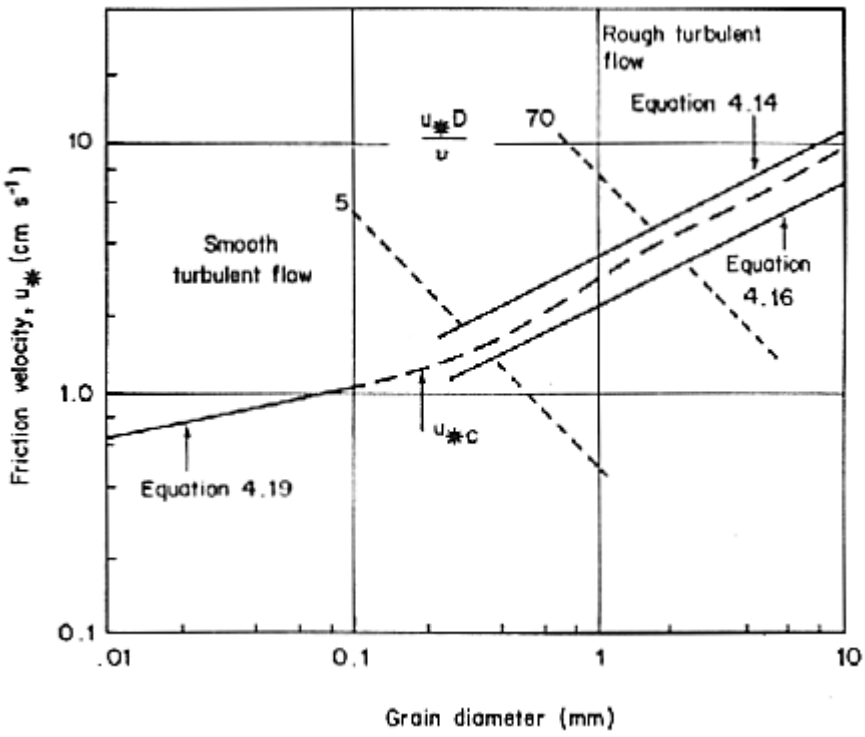

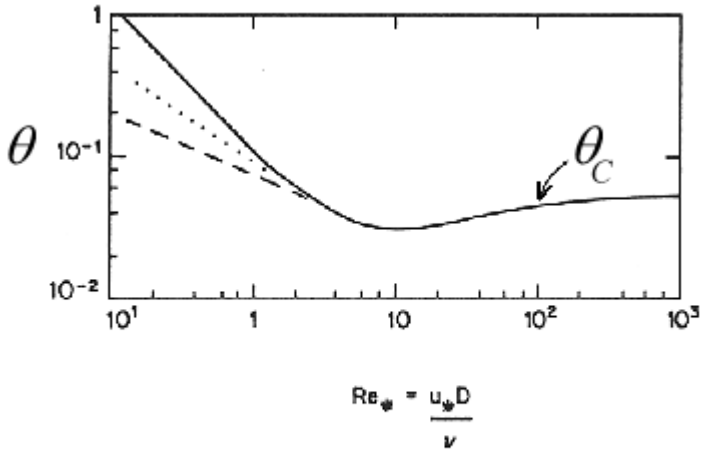

Figure 4.8 Shields threshold curve, solid line, compared with the results of White (1970), dashed line, and those of Grass (1970), dotted line

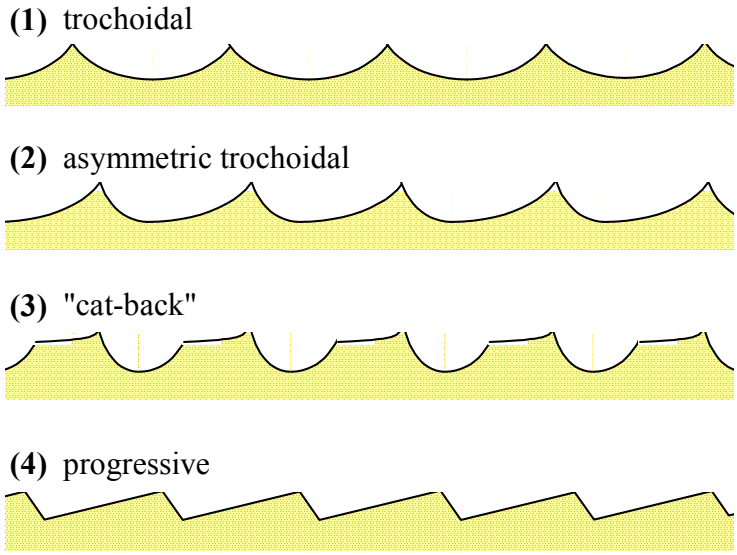

Different shapes of sand-wave fields: Van Deen's Typology
(adapted from Dyer, 1986, p.273; vertical scales are exaggerated)

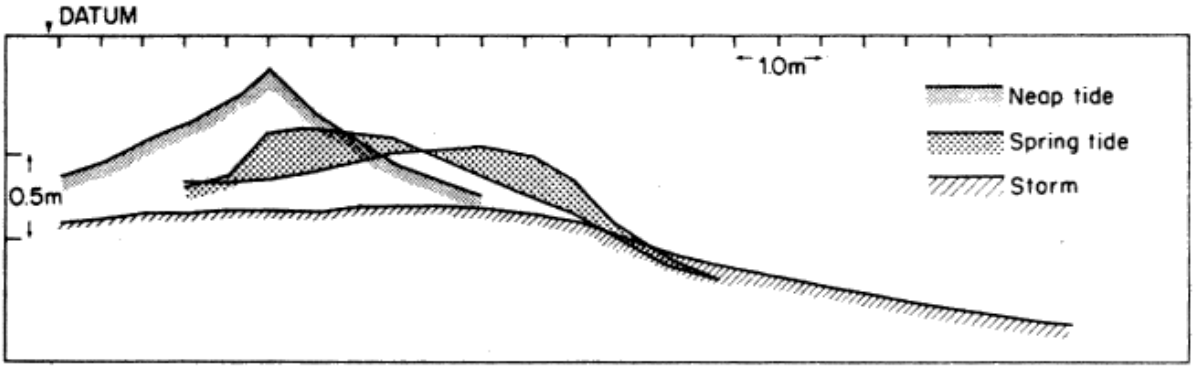

from Dyer, 1986, p.277

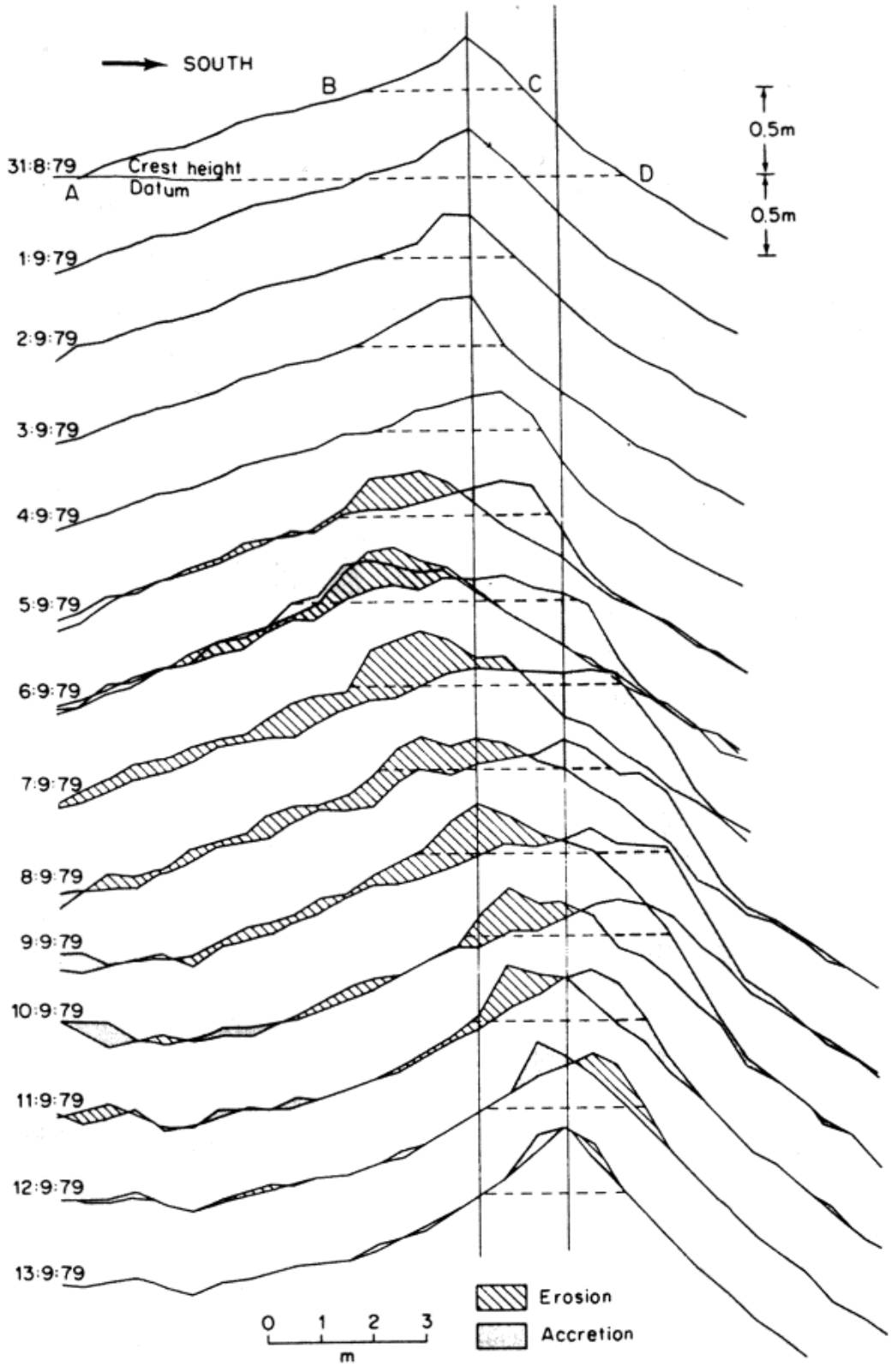

(from Dyer, 1986, p.276)

Some information borrowed from:

H. Chamley ***LES MILIEUX DE SEDIMENTATION ("Sediment Depositional Systems")***
Lavoisier/BRGM, Paris/Orléans, 1986

A famous case of tidal sand-ridges and sand-wave fields (southern North Sea)

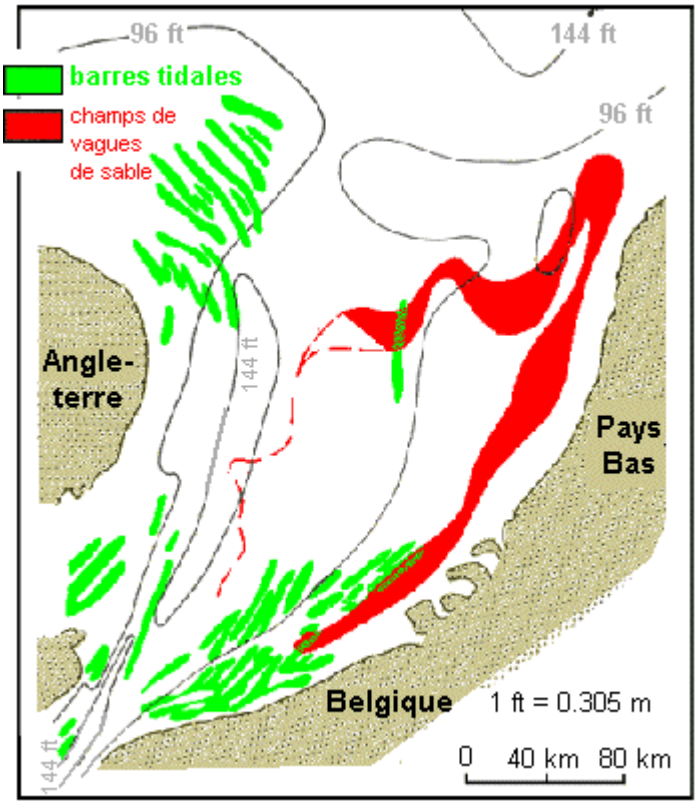

(adapted from Chamley, 1988, p.94)

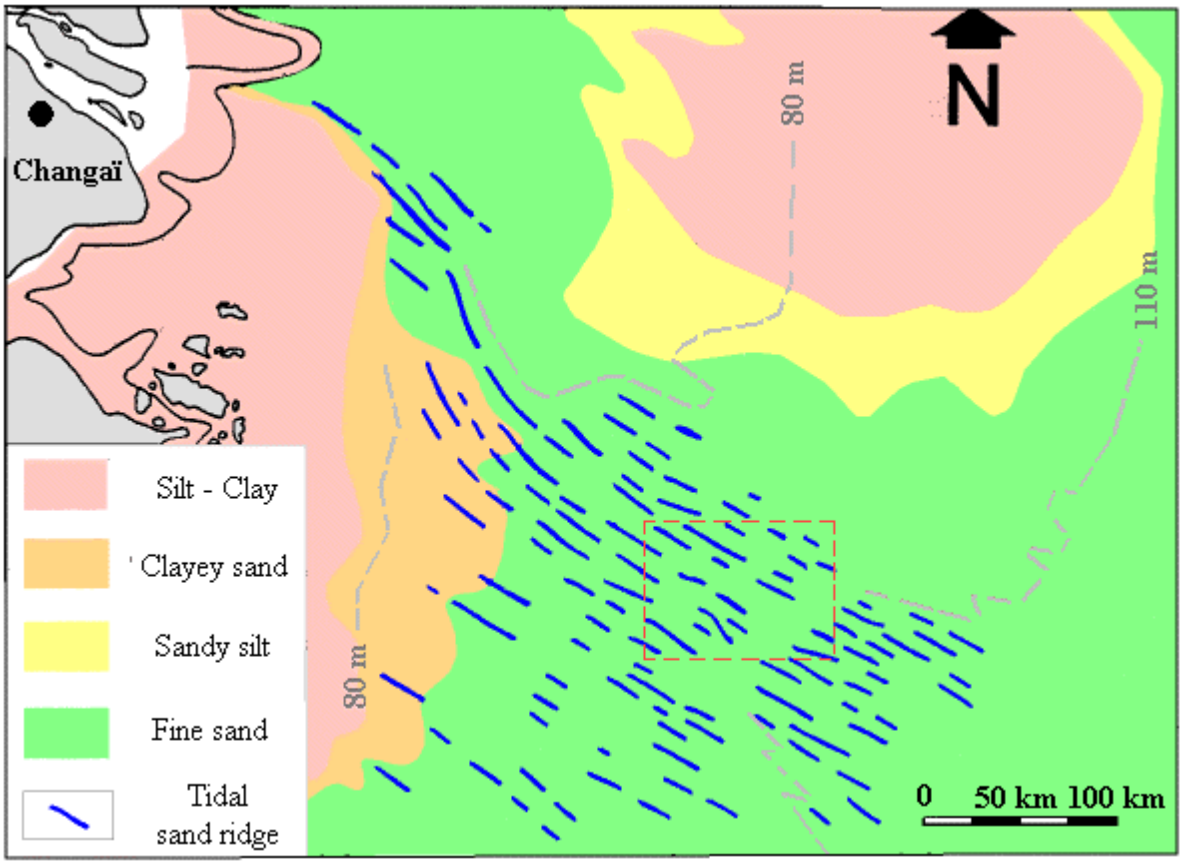

The Continental Shelf off Shang-Hai (Distribution of Bottom natures)

from Y.Chang-Shu & S. Jia-Son *"Tidal Sand Ridges on the East China Sea Shelf"* (p.24), *in* P.L.de Boer, A.van Gelder & S.D. Nio, ed.

TIDE-INFLUENCED SEDIMENTARY ENVIRONMENTS AND FACIES,
D.Reidel Publishing Company, Dordrecht, 1988

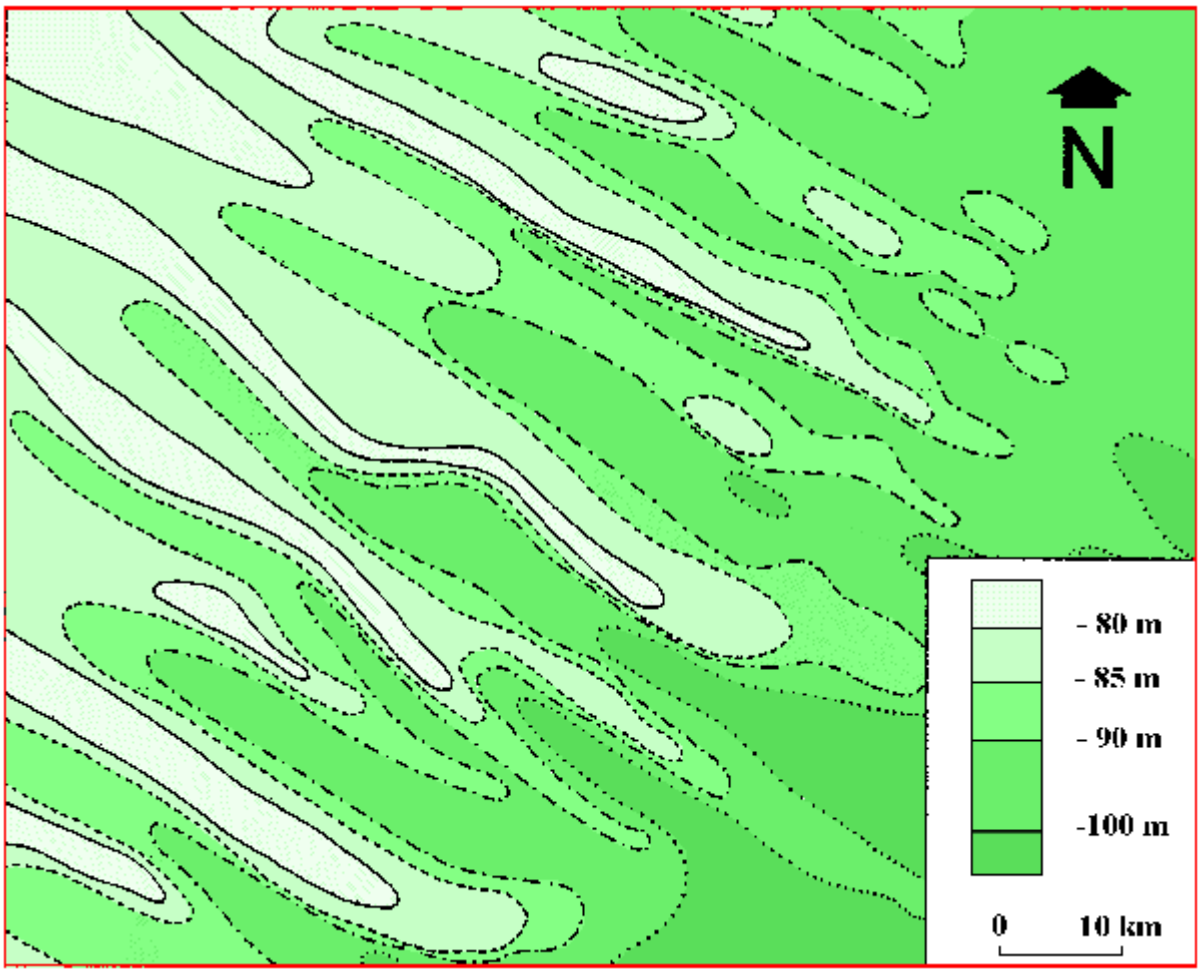

A Close-Up Look at the Field of "Fossile" Sand-Dunes (East of Shang-Hai)

The "fossile" tidal ridges were created by tidal currents interacting with bottom, when the sea level was lower than today. Today's bottom depths and dune ages may be more-or-less associated as follows:

about 100-120m → c.13500 years Before Present
about 80-100 m→ c.12750 years B.P.
about 60-80 m → c.12000 years B.P.
about 50-60 m → c.11000 years B.P.

The ridges are conserved at the water's contact due to low currents at their recent depths.

from Y.Chang-Shu & S. Jia-Son *"Tidal Sand Ridges on the East China Sea Shelf"* (p.25), *in* P.L.de Boer, A.van Gelder & S.D. Nio, ed.

TIDE-INFLUENCED SEDIMENTARY ENVIRONMENTS AND FACIES,
D.Reidel Publishing Company, Dordrecht, 1988

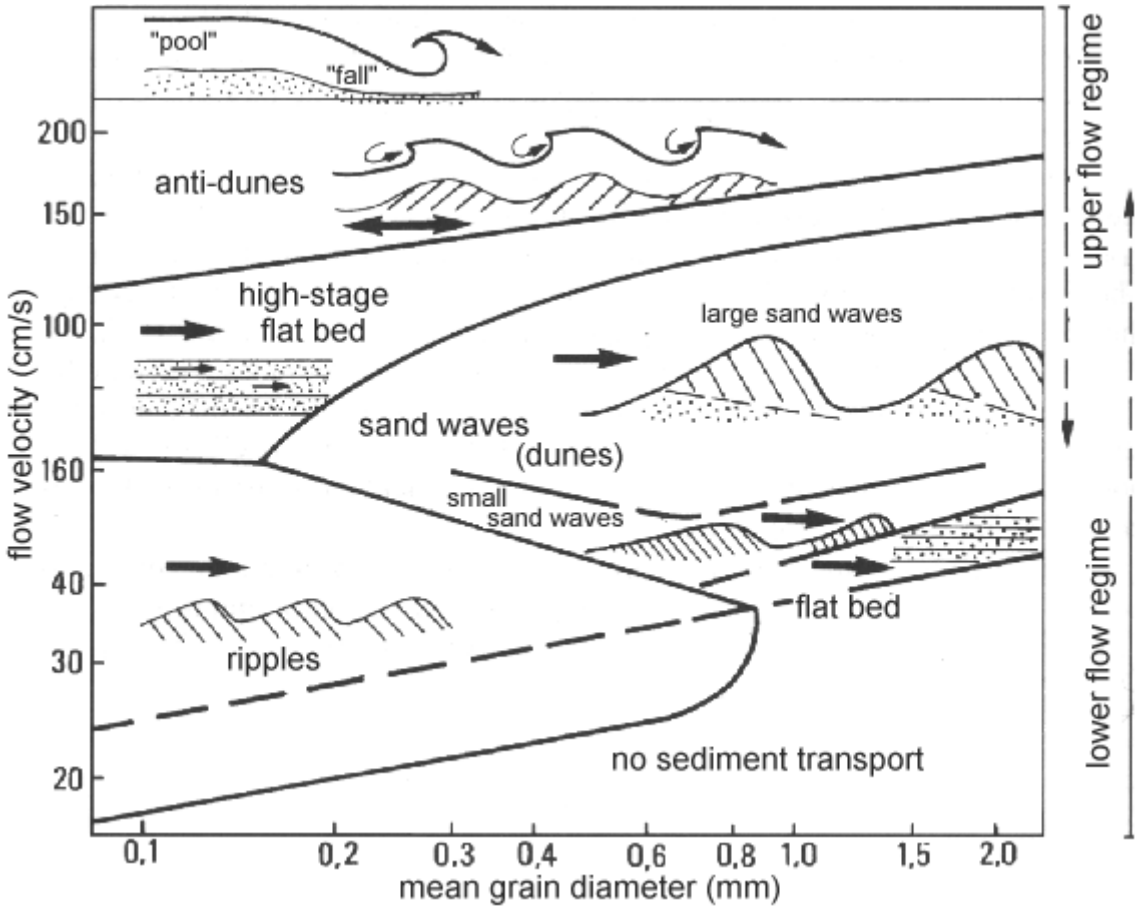

Different sediment regimes in unidirectional flow (adapted from Chamley, 2000)

References

[1] A. Ishimaru. *Wave Propagation and Scattering in Random Media*. Academic Press, 1978.

[2] K.V. Mackenzie. Bottom reverberation for 530 and 1030 cps sound in deep water. *Journal of the Acoustical Society of America*, 33:1498–1504, November 1961.

[3] T. Garlan and X. Demoulin. Sedimentological acoustics: an attempt to reduce the gap between acoustical modelling and sedimentological survey. In *High Frequency Acoustics in Shallow Water*, SACLANTCEN conference Proceedings Series CP-45, 1997.

[4] D.D. Ellis and D.V. Crowe. Bistatic reverberation calculations using a three-dimensional scattering function. *Journal of the Acoustical Society of America*, 89(5):2207–2214, May 1991.

[5] University of Birmingham. *Sonar course, Portland Heights*. U. of Birmingham, 1989.

[6] H.H. Essen. Scattering from a rough sedimental seafloor containing shear and layering. *Journal of the Acoustical Society of America*, 95(3):1299–1310, March 1994.

[7] J.M. Hovem. *Marin akustikk, del II*. Tapir, 2000.

[8] R.J. Urick. *Principles of Underwater Sound*. McGraw Hill, 3rd edition, 1983.

[9] I. Preston, Kinney, and Jespers. Estimates of monostatic and bistatic reverberation using low-frequency linear fm pulses. Technical Report SR-182, SACLANTCEN, 1991.

[10] D.R Del Balzo, J.H. Leclere, and M.J. Collins. Critical angle and seabed scattering issues for active-sonar performance predictions in shallow water. In *High Frequency Acoustics in Shallow Water*, SACLANTCEN conference Proceedings Series CP-45, 1997.

[11] J.A. Ogilvy. *Theory of wave scattering from random rough surfaces*. IOP Publishing, Philadelphia, 1991.

[12] J.W. Caruthers and J.C. Novarini. Modeling bistatic bottom scattering strength including a forward scatter lobe. *IEEE J. Oceanic Eng.*, 18(2):100–107, April 1993.

[13] J.C. Novarini and J.W. Caruthers. The partition wavenumber in acoustic backscattering from a two-scale rough surface described by a power law spectrum. *IEEE J. Oceanic Eng.*, 19(2):200–207, April 1994.

[14] J.C. Novarini and J.W. Caruthers. A simplified approach to backscattering from a rough seafloor with sediment inhomogeneities. *IEEE J. Oceanic Eng.*, 23(3):157–166, July 1998.

[15] H. Weinberg. Generic sonar model. Technical Report TD5971D, NUSC, 1985.

[16] X. Christol. Final Stochastic Model. Technical report, SWAN-MAST-III Project, 2000.

[17] A.P. Lyons and A.L. Anderson. Acoustic scattering from the seafloor: Modeling and data comparison. *Journal of the Acoustical Society of America*, 95(5):2441–2451, May 1994.

[18] T. Yamamoto. Acoustic scattering in the ocean from velocity and density fluctuations in the sediment. *Journal of the Acoustical Society of America*, 99(2):866–879, February 1996.

[19] C.M. McKinney and C.D. Anderson. Measurements of backscattering of sound from the ocean bottom. *Journal of the Acoustical Society of America*, 36(1):158–163, January 1964.

[20] X. Christol. TMS scatter index model. Private communication.

[21] S.A. Frivik. A study on the possibility of using angle dependent acoustic backscattering strength data for seafloor classification. Technical Report NO 429810, NTNU, 1998.

DISTRIBUTION LIST

FFIBM **Dato:** 12 September 2001

RAPPORTTYPE (KRYSS AV)	RAPPORT NR.	REFERANSE	RAPPORTENS DATO
X RAPP ☐ NOTAT ☐ RR	2001/03685	FFIBM/821/116	12 September 2001
RAPPORTENS BESKYTTELSESGRAD		ANTALL EKS UTSTEDT	ANTALL SIDER
Unclassified		30	55
RAPPORTENS TITTEL		FORFATTER(E)	
RUMBLE PROJECT SCATTERING INDEX MODELS		JENSERUD Trond , FFIBM, NO SIMONS Dick, TNO-FEL, NL CRISTOL Xavier, TMS, FR	
FORDELING GODKJENT AV FORSKNINGSSJEF:		FORDELING GODKJENT AV AVDELINGSSJEF:	

EKSTERN FORDELING

ANTALL	EKS NR	TIL
1		IA Erwan BERNI (Chairman) DGA/DSA/SPN/ST/LSM 8, Bd Victor 00303 PARIS ARMEES, France
1		LCDR Peer TAS MSc Directorate of Material Royal Netherlands Navy Department of Weapon and Communication Systems Underwater Sensor- and Weapon Systems branch Van der Burchlaan 31, P.O. Box 20702 2500 ES The Hague, The Netherlands
1		Wessel GROOT WEAO Research Cell Rue de la Régence 4 1000 BRUXELLES, Belgique
1		Alain PLAISANT THOMSON MARCONI SONAR 525 Route des Dolines BP 157, Valbonne 06903 SOPHIA ANTIPOLIS Cedex France
1		Arne LØVIK Kongsberg Defence Aerospace P.O. Box 55, 7501 Stjørdal
1		Johnny DYBEDAL Kongsberg Defence Aerospace P.O. Box 55 7501 Stjørdal
1		Dick SIMONS TNO – FEL Oude Waalsdorperweg 63 P.O. Box 96864 2509 JG The Hague, The Netherlands

INTERN FORDELING

ANTALL	EKS NR	TIL
14		FFI-Bibl
1		Adm direktør/stabssjef
1		FFIE
1		FFISYS
1		FFIBM
1		FFIN
1		Forfattereksemplar(er):
2		Restopplag til FFI-Bibl
1		Avd ktr FFIBM/Horten
		Elektronisk fordeling:
		FFI-veven
		Jarl K.Johnsen (JKJ)
		Tor Knudsen (TKn)
		Trond Jenserud (TJe)
		Yngvar Nustad (YNu)
		Erik Sevaldsen (ESe)
		Elin M. Dombestein (EMD)
		Elling Tveit (ETv)
		Dag Tollefsen (DTo)

FFI-K1 Retningslinjer for fordeling og forsendelse er gitt i Oraklet, Bind I, Bestemmelser om publikasjoner for Forsvarets forskningsinstitutt, pkt 2 og 5. Benytt ny side om nødvendig.